

AD A109476

OFFICE OF NAVAL RESEARCH

Contract N00014-76-C-0817

Task No. Nr 359-623

TECHNICAL REPORT NO. 20

LEVEL II

12

PERMEATION OF ELECTROACTIVE SOLUTES THROUGH ULTRATHIN POLYMERIC FILMS ON
ELECTRODE SURFACES

by

T. Ikeda, R. Schmehl, P. Denisevich, K. Willman and R. W. Murray

Kenan Laboratories of Chemistry

University of North Carolina

Chapel Hill, North Carolina 27514

Prepared for Publication

in the

Journal of the American Chemical Society

Kenan Laboratories of Chemistry

University of North Carolina

Chapel Hill, North Carolina 27514

December 18, 1981

Reproduction in whole or in part is permitted for
any purpose of the United States Government

This document has been approved for public release
and sale; its distribution is unlimited

DTIC
ELECTE
JAN 08 1982
S **D**
E

DTIC FILE COPY

REPORT DOCUMENTATION PAGE		READ INSTRUCTIONS BEFORE COMPLETING FORM
1. REPORT NUMBER TWENTY	2. GOVT ACCESSION NO. AD-A109476	3. RECIPIENT'S CATALOG NUMBER
4. TITLE (and Subtitle) PERMEATION OF ELECTROACTIVE SOLUTES THROUGH ULTRATHIN POLYMERIC FILMS ON ELECTRODE SURFACES		5. TYPE OF REPORT & PERIOD COVERED Technical Report
		6. PERFORMING ORG. REPORT NUMBER 111-20
7. AUTHOR(s) T. Ikeda, R. Schmehl, P. Denisevich, K. Willman and Royce W. Murray		8. CONTRACT OR GRANT NUMBER(s) N00014-76-C-0817
9. PERFORMING ORGANIZATION NAME AND ADDRESS Department of Chemistry University of North Carolina Chapel Hill, North Carolina 27514		10. PROGRAM ELEMENT, PROJECT, TASK AREA & WORK UNIT NUMBERS
11. CONTROLLING OFFICE NAME AND ADDRESS Office of Naval Research Department of the Navy Arlington, Virginia 22217		12. REPORT DATE December 18, 1981
		13. NUMBER OF PAGES 56
14. MONITORING AGENCY NAME & ADDRESS (if different from Controlling Office)		15. SECURITY CLASS. (of this report) Unclassified
		15a. DECLASSIFICATION/DOWNGRADING SCHEDULE
15. DISTRIBUTION STATEMENT (of this Report) Approved for Public Release, Distribution Unlimited		
17. DISTRIBUTION STATEMENT (of the abstract entered in Block 20, if different from Report)		
18. SUPPLEMENTARY NOTES		
19. KEY WORDS (Continue on reverse side if necessary and identify by block number) membrane, diffusion, permeation, electrode, polymer film, ruthenium, electropolymerization		
20. ABSTRACT (Continue on reverse side if necessary and identify by block number) The rates of permeation of a series of electroactive solutes, bromide, ferrocene, benzoquinone, diquat, $[\text{Ru}(\text{bpy})_2\text{Cl}_2]$, $[\text{Fe}(\text{bpy})_2(\text{CN})_2]$, and $[\text{Ru}(\text{bpy})_2(\text{py})\text{Cl}]^+$ have been measured through ultrathin, electrochemically polymerized films like poly- $[\text{Ru}(\text{vbpy})_3]^{2+}$. The films are coated on Pt disk electrodes. The permeabilities, expressed as $\text{PD}_{\text{S, pol}}$, the product of a partition coefficient and a diffusion coefficient in the film, range from very fast (bromide, $> 4 \times 10^{-7} \text{ cm}^2/\text{sec.}$). The permeation rates vary linearly with film thickness; this and the molecular size discrimination rule out transport through larger-than-molecular-dimensional channels and pinholes in (over)		

✓ BLOCK #20, ABSTRACT, continued:

the film. The film permeability process is described as membrane diffusion. Relatively pinhole-free films are preparable as thin as 20 - 40 Å.

angstroms
af

TECHNICAL REPORT DISTRIBUTION LIST, GEN

	<u>No. Copies</u>		<u>No. Copies</u>
Office of Naval Research Attn: Code 472 800 North Quincy Street Arlington, Virginia 22217	2	U.S. Army Research Office Attn: CRD-AA-IP P.O. Box 1211 Research Triangle Park, N.C. 27709	1
ONR Western Regional Office Attn: Dr. R. J. Marcus 1030 East Green Street Pasadena, California 91106	1	Naval Ocean Systems Center Attn: Mr. Joe McCartney San Diego, California 92152	1
ONR Eastern Regional Office Attn: Dr. L. H. Peebles Building 114, Section D 666 Summer Street Boston, Massachusetts 02210	1	Naval Weapons Center Attn: Dr. A. B. Amster, Chemistry Division China Lake, California 93555	1
Director, Naval Research Laboratory Attn: Code 6100 Washington, D.C. 20390	1	Naval Civil Engineering Laboratory Attn: Dr. R. W. Drisko Port Hueneme, California 93401	1
The Assistant Secretary of the Navy (RE&S) Department of the Navy Room 4E736, Pentagon Washington, D.C. 20350	1	Department of Physics & Chemistry Naval Postgraduate School Monterey, California 93940	1
Commander, Naval Air Systems Command Attn: Code 310C (H. Rosenwasser) Department of the Navy Washington, D.C. 20360	1	Scientific Advisor Commandant of the Marine Corps (Code RD-1) Washington, D.C. 20380	1
Defense Technical Information Center Building 5, Cameron Station Alexandria, Virginia 22314	12	Naval Ship Research and Development Center Attn: Dr. G. Bosmajian, Applied Chemistry Division Annapolis, Maryland 21401	1
Dr. Fred Smalfield Chemistry Division, Code 6100 Naval Research Laboratory Washington, D.C. 20375	1	Naval Ocean Systems Center Attn: Dr. S. Yamamoto, Marine Sciences Division San Diego, California 91232	1
		Mr. John Boyle Materials Branch Naval Ship Engineering Center Philadelphia, Pennsylvania 19112	1

Accession For	NTIS GRA&I	<input checked="" type="checkbox"/>	<input type="checkbox"/>
	DTIC TAB	<input type="checkbox"/>	<input type="checkbox"/>
	Unannounced		
	Justification		
By	Distribution/		
	Availability Codes		
	Avail and/or		
Dist	Special		

A

TECHNICAL REPORT DISTRIBUTION LIST, 359

	<u>No. Copies</u>		<u>No. Copies</u>
Dr. Paul Delahay Department of Chemistry ✓ New York University New York, New York 10003	1	Dr. P. J. Hendra Department of Chemistry University of Southampton Southampton SO9 5NH United Kingdom	1
Dr. E. Yeager Department of Chemistry Case Western Reserve University Cleveland, Ohio 44106	1	Dr. Sam Perone Department of Chemistry Purdue University West Lafayette, Indiana 47907	1
Dr. D. N. Bennion Department of Chemical Engineering ✓ Brigham Young University Provo, Utah 84602	1	Dr. Royce W. Murray Department of Chemistry University of North Carolina Chapel Hill, North Carolina 27514	1
Dr. R. A. Marcus Department of Chemistry California Institute of Technology Pasadena, California 91125	1	Naval Ocean Systems Center Attn: Technical Library San Diego, California 92152	1
Dr. J. J. Auburn ✓ Bell Laboratories Murray Hill, New Jersey 07974	1	Dr. C. E. Mueller The Electrochemistry Branch Materials Division, Research & Technology Department Naval Surface Weapons Center White Oak Laboratory Silver Spring, Maryland 20910	1
Dr. Adam Heller Bell Laboratories Murray Hill, New Jersey 07974	1	Dr. G. Goodman Globe-Union Incorporated 5757 North Green Bay Avenue Milwaukee, Wisconsin 53201	1
Dr. T. Katan Lockheed Missiles & Space Co, Inc. P.O. Box 504 Sunnyvale, California 94088	1	Dr. J. Boechler Electrochimica Corporation Attention: Technical Library 2485 Charleston Road Mountain View, California 94040	1
Dr. Joseph Singer, Code 302-1 NASA-Lewis 21000 Brookpark Road Cleveland, Ohio 44135	1	Dr. P. P. Schmidt ✓ Department of Chemistry Oakland University Rochester, Michigan 48063	1
Dr. B. Brummer EIC Incorporated 55 Chapel Street Newton, Massachusetts 02158	1	Dr. H. Richtol ✓ Chemistry Department Rensselaer Polytechnic Institute Troy, New York 12181	1
Library P. R. Mallory and Company, Inc. Northwest Industrial Park Burlington, Massachusetts 01803	1		

TECHNICAL REPORT DISTRIBUTION LIST, 359

	<u>No. Copies</u>		<u>No. Copies</u>
Dr. A. B. Ellis Chemistry Department University of Wisconsin Madison, Wisconsin 53706	1	Dr. R. P. Van Duyne Department of Chemistry Northwestern University Evanston, Illinois 60201	1
Dr. M. Wrighton Chemistry Department Massachusetts Institute of Technology Cambridge, Massachusetts 02139	1	Dr. B. Stanley Pons Department of Chemistry ✓ University of Alberta Edmonton, Alberta CANADA T6G 2G2	1
Larry E. Plew Naval Weapons Support Center Code 30736, Building 2906 Crane, Indiana 47522	1	Dr. Michael J. Weaver Department of Chemistry Michigan State University East Lansing, Michigan 48824	1
S. Rubv DOE (STOR) 600 E Street Washington, D.C. 20545	1	Dr. R. David Rauh EIC Corporation 55 Chapel Street Newton, Massachusetts 02158	1
Dr. Aaron Wold Brown University Department of Chemistry Providence, Rhode Island 02192	1	Dr. J. David Margerum Research Laboratories Division ✓ Hughes Aircraft Company 3011 Malibu Canyon Road Malibu, California 90265	1
Dr. R. C. Chudacek McGraw-Edison Company Edison Battery Division Post Office Box 28 Bloomfield, New Jersey 07003	1	Dr. Martin Fleischmann Department of Chemistry University of Southampton Southampton 509 5NH England	1
Dr. A. J. Bard University of Texas Department of Chemistry Austin, Texas 78712	1	Dr. Janet Osteryoung Department of Chemistry ✓ State University of New York at Buffalo Buffalo, New York 14214	1
Dr. M. M. Nicholson Electronics Research Center Rockwell International 3370 Miraloma Avenue Anaheim, California	1	Dr. R. A. Osteryoung Department of Chemistry ✓ State University of New York at Buffalo Buffalo, New York 14214	1
Dr. Donald W. Ernst Naval Surface Weapons Center Code R-33 White Oak Laboratory Silver Spring, Maryland 20910	1	Mr. James R. Moden ✓ Naval Underwater Systems Center Code 3632 Newport, Rhode Island 02840	1

TECHNICAL REPORT DISTRIBUTION LIST, 359

	<u>No.</u> <u>Copies</u>		<u>No.</u> <u>Copies</u>
Dr. R. Nowak Naval Research Laboratory Code 6130 Washington, D.C. 20375	1	Dr. Bernard Spielvogel U.S. Army Research Office P.O. Box 12211 Research Triangle Park, NC 27709	1
Dr. John F. Houlihan Shenango Valley Campus Pennsylvania State University Sharon, Pennsylvania 16146	1	Dr. Denton Elliott Air Force Office of Scientific Research Bolling AFB Washington, DC 20332	1
Dr. D. F. Shriver Department of Chemistry Northwestern University Evanston, Illinois 60201	1	Dr. David Aikens Chemistry Department Rensselaer Polytechnic Institute Troy, NY 12181	1
Dr. D. H. Whitmore Department of Materials Science Northwestern University Evanston, Illinois 60201	1	Dr. A. P. B. Lever Chemistry Department York University Downsview, Ontario M3J1P3 Canada	1
Dr. Alan Bewick Department of Chemistry The University Southampton, SO9 5NH England	1	Mr. Maurice F. Murphy Naval Sea Systems Command 63R32 2221 Jefferson Davis Highway Arlington, VA 20360	1
Dr. A. Himy NAVSEA-5433 NC #4 2541 Jefferson Davis Highway Arlington, Virginia 20362	1	Dr. Stanislaw Szpak Naval Ocean Systems Center Code 6343 San Diego, CA 95152	1
Dr. John Kincaid Department of the Navy Strategic Systems Project Office Room 901 Washington, DC 20376	1	Dr. Gregory Farrington Department of Materials Science & Engineering University of Pennsylvania Philadelphia, PA 19104	1
M. L. Robertson Manager, Electrochemical Power Sonics Division Naval Weapons Support Center Crane, Indiana 47522	1	Dr. Bruce Dunn Department of Engineering & Applied Science University of California Los Angeles, CA 90024	1
Dr. Elton Cairns Energy & Environment Division Lawrence Berkeley Laboratory University of California Berkeley, California 94720	1		

TECHNICAL REPORT DISTRIBUTION LIST, 359No.
Copies

Dr. Micha Tomkiewicz
Department of Physics
Brooklyn College
Brooklyn, NY 11210

1

Dr. Lesser Blum
Department of Physics
University of Puerto Rico
Rio Piedras, PR 00931

1

Dr. Joseph Gordon II
IBM Corporation
K33/281
5600 Cottle Road
San Jose, CA 95193

1

Dr. Robert Somoano
Jet Propulsion Laboratory
California Institute of Technology
Pasadena, CA 91103

1

RECEIVED 12/81

PERMEATION OF ELECTROACTIVE SOLUTES THROUGH ULTRATHIN POLYMERIC FILMS
ON ELECTRODE SURFACES

T. Ikeda*, R. Schmehl, P. Denisevich, K. Willman and R. W. Murray*

Kenan Laboratories of Chemistry

University of North Carolina

Chapel Hill, North Carolina 27514

ABSTRACT

The rates of permeation of a series of electroactive solutes, bromide, ferrocene, benzoquinone, diquat, $[\text{Ru}(\text{bpy})_2\text{Cl}_2]$, $[\text{Fe}(\text{bpy})_2(\text{CN})_2]$, and $[\text{Ru}(\text{bpy})_2(\text{py})\text{Cl}]^+$ have been measured through ultrathin, electrochemically polymerized films like $\text{poly}[\text{Ru}(\text{vbpy})_3]^{2+}$. The films are coated on Pt disk electrodes. The permeabilities, expressed as $\text{PD}_{\text{S, pol}}$, the product of a partition coefficient and a diffusion coefficient in the film, range from very fast (bromide, $> 4 \times 10^{-7} \text{ cm}^2/\text{sec.}$) to measurable and sensitive to solute size and charge ($2 - 58 \times 10^{-9} \text{ cm}^2/\text{sec.}$) to immeasurably slow ($[\text{Ru}(\text{bpy})_2(\text{py})\text{Cl}]^+$, $< 7 \times 10^{-12} \text{ cm}^2/\text{sec.}$). The permeation rates vary linearly with film thickness; this and the molecular size discrimination rule out transport through larger-than-molecular-dimensional channels and pinholes in the film. The film permeability process is described as membrane diffusion. Relatively pinhole-free films are preparable as thin as 20 - 40 Å.

PERMEATION OF ELECTROACTIVE SOLUTES THROUGH ULTRATHIN POLYMERIC FILMS ON ELECTRODE SURFACES

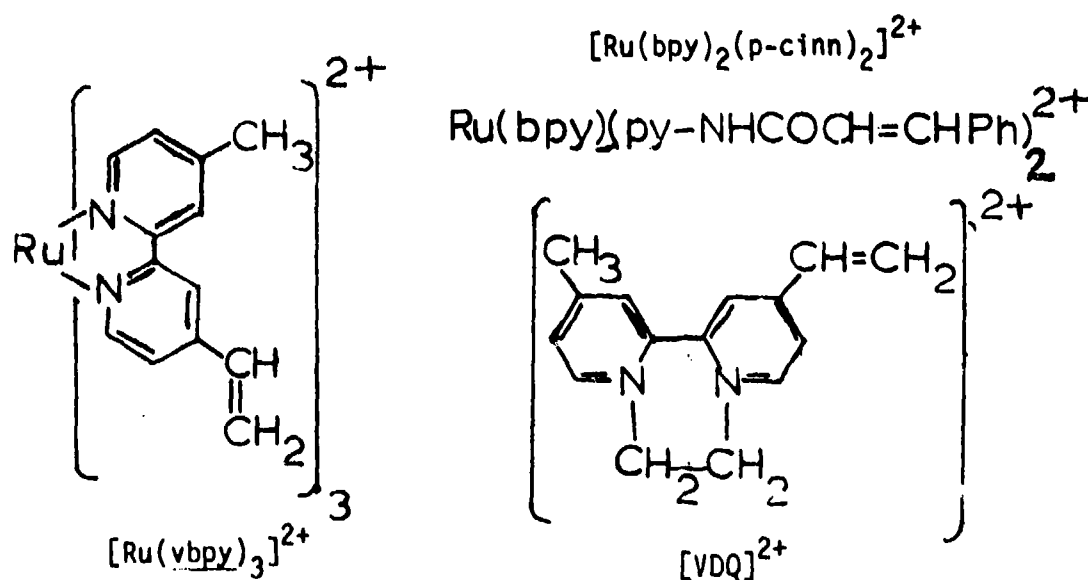
T. Ikeda^{*1}, R. Schmehl, P. Denisevich, K. Willman and R. W. Murray^{*}

Kenan Laboratories of Chemistry

University of North Carolina

Chapel Hill, North Carolina 27514

This paper describes electrochemical reactions of acetonitrile solutions of electroactive species at electrodes covered with very thin films (ca. 20 to 450 Å) of redox polymers. Specifically, rates of permeation of electroactive solutes through redox polymer films to the electrode have been measured as a function of film polymeric structure and of solute size and charge. The polymer coated Pt electrodes are prepared by polymerization-inducing reductions of the electroactive monomers¹⁻⁵



¹Department of Agricultural Chemistry, Kyoto University, Kyoto, Japan

in acetonitrile and are abbreviated Pt/poly-[Ru(vbpy)₃]²⁺, Pt/poly-[Ru(bpy)₂(p-cinn)₂]²⁺, and Pt/poly-VDQ²⁺, where bpy is 2,2'-bipyridine and p-cinn is N-(4-pyridyl)cinnamide.

The electroactive solutes are p-benzoquinone, ferrocene, diquat (DQ²⁺; N,N'-ethylene-2,2'-bipyridine), [Ru(bpy)₂Cl₂], [Fe(bpy)₂(CN)₂], [Ru(bpy)₃]²⁺, and [Ru(bpy)₂(py)Cl]⁺. Permeabilities of all solutes except [Ru(bpy)₃]²⁺ were evaluated for the Pt/poly-[Ru(vbpy)₃]²⁺ films, while for Pt/poly-[Ru(bpy)₂p-cinn)₂]²⁺, ferrocene and [Ru(bpy)₂Cl₂] solutions were studied, and for Pt/poly-VDQ²⁺, solutions of ferrocene, [Ru(bpy)₂Cl₂], and [Ru(bpy)₃]²⁺. The solute permeabilities at film coated rotated disk electrodes were determined from the variations of their limiting currents with electrode rotation rate ω and film thickness.

Thorough understanding of solute transport through thin films is important in describing the catalytic or inhibitory behavior of such films. Solute permeation is relevant to processes in ultrathin films, phases, and membranes such as phospholipid bilayer membranes⁶, biological cell walls⁷, supported oriented-monolayer films⁶, drug encapsulation polymers⁸, immobilized enzyme systems⁹, zeolite particles^{10,11}, surfactant micellar¹² and vesicle^{13,14} structures, and corrosion-inhibiting films on metals, electronic microcircuits, and semiconductor electrodes. The actual transport constants are in most cases, however, unmeasured, one difficulty being that of preparing ultrathin films in suitable physical forms and another being that of distinguishing transport as a solute "dissolved" in the film (which we shall term membrane diffusion) from transport through film imperfections (pinhole and channel diffusion).

Transport of solutes through redox polymer coated electrodes is important in their applications to electrocatalysis¹⁵⁻³⁹ and photoelectrochemistry⁴⁰⁻⁴³ and in relation to the transport of electrochemical charge through such polymers which occurs via electron self-exchange

reactions of the redox sites^{22,39,41,44-52}. Film permeability is of particular interest with respect to the evolving theory^{32-39,44} of mediated electrocatalysis. Again, the transport data available^{17,19,21} to address these problems quantitatively are very limited, and there has been no study of the variation of permeability with either solute or film structure.

Our experiences with electrochemically prepared redox polymer films as used in bilayer film electrodes^{1,2} suggest that these films are often free of imperfections even when the film contains only 5-10 layers of redox monomer sites. It is furthermore possible to systematically vary the thickness d of these films as measured in mol./cm^2 , Γ_T , of ruthenium (III/II) and $\text{VDQ}^{2+/1+}$ redox sites. Γ_T is determined from voltammetry of the film in monomer free solution. The films thus represent an opportunity to address the difficult issue¹⁷ of film imperfections and to systematically examine structural effects on ultra-thin film transport.

EXPERIMENTAL

Electrochemical Polymerization of Redox Polymer Films on Electrodes.

Synthesis of the electroactive monomers $[\text{Ru}(\text{vbpy})_3]^{2+}$, $[\text{Ru}(\text{bpy})_2(\text{p-cinn})_2]^{2+}$, and VDQ^{2+} , details of their reductions to form polymer films on electrodes, electrochemical properties of the films and the kinetics of their electron transfer mediation reactions with several electroactive solutes are described elsewhere^{3-5,33,53}. Briefly, to prepare a film, the potential applied to a Teflon-shrouded Pt disk electrode is swept repeatedly between 0 V vs. SSCE and the second of the one-electron monomer reduction waves in 0.1, 0.5, and 1 mM thor-

oughly-degassed acetonitrile solutions of the three monomers, respectively. The thickness of the polymer films built up in this manner increases linearly with the number of repetitive potential sweeps³, as assessed by the increasing peak currents for the two reduction waves of still-electroactive, polymerized monomer, and more quantitatively by the charge under slow potential scan cyclic voltammetric waves for the $\text{Ru}^{\text{III/II}}$ and $\text{VDQ}^{2+/1+}$ couple waves in monomer free acetonitrile solution. Permeability results include data for electrodes prepared as a group and bearing a series of film thicknesses, as well as data from individual electrodes prepared over a period of several months. Following film deposition, electrodes were thoroughly rinsed with acetonitrile and carefully stored in air in a closed vial. To minimize the incidence of film imperfections caused by handling, films were ordinarily not employed for more than one or two sets of permeability measurements with an electroactive solute.

The Pt/poly- $[\text{Ru}(\text{vbpy})^{2+}]$ /PVFer bilayer electrode was prepared as described elsewhere^{1,2}, by evaporation of a droplet of polyvinylferrocene in toluene solution on the surface of a Pt/poly- $[\text{Ru}(\text{vbpy})_3]^{2+}$ electrode.

Procedure for Permeability Measurement. Permeability measurements were based on the limiting currents of voltammograms of the electrochemical oxidations or reductions of the electroactive solutes at polymer film coated Pt disk electrodes rotated in Pine Instrument Co. Model PIR and NSY assemblies, varying electrode rotation rate over $400\text{--}10^4$ rpm ($\omega^{1/2} = 20\text{--}100$ rpm^{1/2}). Voltammograms for the ruthenium polymer films were extended to include the electron transfer mediated wave for the solute which occurs near the $\text{Ru}^{\text{III/II}}$ potential (vide infra). The acetonitrile

solutions were 0.1 M in Et_4NClO_4 supporting electrolyte, and usually $< 0.5 \text{ mM}$ in electroactive solute. The low solute concentration was chosen to avoid alterations in film swelling, and in the electron transfer mediated wave, to avoid charge transport rate limitations in the polymer films⁵³.

Electrochemical Equipment and Chemicals. $[\text{Ru}(\text{bpy})_2\text{Cl}_2]$ and $[\text{Fe}(\text{bpy})_2(\text{CN})_2]$ were synthesized by literature procedures^{54,55}; ferrocene (Aldrich) was used as received, and p-benzoquinone (J. T. Baker) after sublimation. Electrochemical equipment and cells were conventional. All potentials are referenced against a NaCl-saturated SCE, designated SSCE.

RESULTS AND DISCUSSION

Membrane Diffusion Theory for Rotated Disk Electrode. The limiting current i_l for electrochemical reaction of a solute which partitions into (with coefficient P) and diffuses to a rotated disk electrode through a membrane barrier with diffusion constant $D_{S,\text{pol}}$ (different from that in the solution D_S) is described by the equation⁵⁶

$$\frac{1}{i_l} = \frac{1}{nFAD_{S,\text{pol}}PC_S/d} + \frac{1}{0.62nFAD_S^{2/3}\nu^{-1/6}\omega^{1/2}C_S} \quad (1)$$

where d is membrane thickness and ω is in rad./sec. The two terms on the right hand side of equation 1 represent respectively the rates of solute diffusion through the membrane and through the Levich depletion layer in solution. If $D_S^{2/3}\nu^{-1/6}\omega^{1/2} \ll PD_{S,\text{pol}}/d$ (e.g., very thin film or large $PD_{S,\text{pol}}$), the diffusion through the Levich layer is the slower of the two and a ("Levich")

plot of i_p vs. $\omega^{1/2}$ is linear with zero intercept. If diffusion through the membrane is slower, the Levich plot is not linear, but a plot of i_p vs. $\omega^{-1/2}$ (an "inverse Levich plot"), is and $PD_{S,pol}/d$ can be evaluated from its intercept.

Important features of an inverse Levich plot are: (i) its slope should yield the same D_S as observed at a naked rotated Pt disk electrode, independent of C_S or d , (ii) the intercept should be inversely proportional to C_S , and (iii) the intercept should be proportional to d (and accordingly Γ_T for the redox polymer films). The latter, vital criterion has not been satisfactorily examined for membrane coated rotated disks.

We should note that membrane diffusion is only one of four conceivable modes of reaction of an electroactive solute at a polymer film coated electrode. The other three are¹⁷: (a) electronic conductivity of the film leading to electrolysis of the solute at the film/solution interface, (b) oxidation or reduction of the solute by electron transfer mediation by redox sites in the polymer film, and (c) diffusion of the electroactive solute through the solvent in film imperfections (channels and pinholes with dimensions much larger than that of the solute or of monomer sites in the film). Experimental results ruling out these three alternative processes will be identified as we come to them.

Poly-[Ru(vbpy)₃]²⁺ and poly-[Ru(bpy)₂(p-cinn)₂]²⁺ films. Electro-reductive polymerization of vinyl monomers like [Ru(vbpy)₃]²⁺ in acetonitrile produces³ an adherent, intractably insoluble polymeric film of the complex on the electrode surface which undergoes electron transfer reactions at potentials similar to those of the monomer, Figure 1, Curve

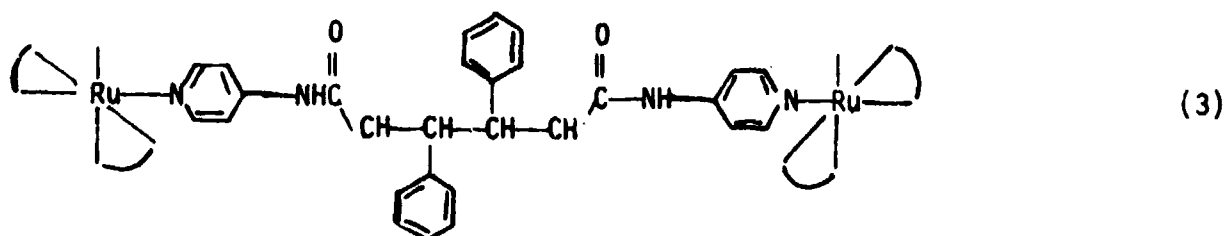
A. The polymerization is rationalized by the thesis^{1,3} that the metal complex reductions are ligand localized, and that radical ions of such activated olefins are prone to coupling and polymer-forming reactions. In an investigation into the generality of this chemistry we have established⁴ that one and (more rapidly) two electron reductions of the monomer $[\text{Ru}(\text{bpy})_2(\text{p-cinn})_2]^{2+}$ also produce stable, adherent redox polymer films which are electroactive as shown in Figure 1, Curve B.

Spectroelectrochemical experiments show² that the electrochemical charge under a slow potential scan poly- $[\text{Ru}(\text{vbpy})_3]^{3+/2+}$ cyclic voltammogram, Figure 1, Curve A, measures all of the film's redox sites, Γ_T , mol./cm². Over the range $\Gamma_T = 10^{-10}$ to 10^{-8} mol./cm², the poly- $[\text{Ru}(\text{vbpy})_3]^{2+}$ and poly- $[\text{Ru}(\text{bpy})_2(\text{p-cinn})_2]^{2+}$ voltammetric waveshapes remain constant, which implies⁵³ that activity parameter G and correspondingly the density of the charge redox sites do not vary substantially over this range. Accordingly, we assume here that the physical thicknesses of the poly- $[\text{Ru}(\text{vbpy})_3]^{2+}$ and poly- $[\text{Ru}(\text{bpy})_2(\text{p-cinn})_2]^{2+}$ films are proportional to Γ_T . Densities of bulk samples of poly- $[\text{Ru}(\text{vbpy})_3]^{2+}$ and poly- $[\text{Ru}(\text{bpy})_2(\text{p-cinn})_2]^{2+}$ are 1.35 and 1.4 g/cm³, which correspond to concentrations of ruthenium redox sites in the polymer of $C_{\text{Ru}} = 1.5 \times 10^{-3}$ and $C_{\text{Ru}}' = 1.2 \times 10^{-3}$ mol./cm³, respectively. Film thicknesses estimated by $d = \Gamma_T/C_{\text{Ru}}$ and $d = \Gamma_T/C_{\text{Ru}}'$ assume that the ultrathin polymer films swell to the same extent in acetonitrile and the solvents used for the density (flotation) measurement. To avoid this assumption in comparison of equation 1 to film thickness, the membrane permeability results will be expressed as

$$\Gamma_T(\text{PD}_{\text{S,pol}}/d) = \text{PD}_{\text{S,pol}} C_{\text{Ru}} \quad (2)$$

which contains no assumptions about film density.

From substantial differences in polymer film forming rates with the degree of vinyl substitution of otherwise similar complexes (e.g., $[\text{Ru}(\text{vbpy})_3]^{2+}$ vs. $[\text{Ru}(\text{bpy})_2(\text{vbpy})]^{2+}$) which seem best interpreted in steric terms, and from other data, we believe that coupling reactions of sterically bulky vinyl-bipyridine radical anion sites are often terminated at the dimer stage. The poly- $[\text{Ru}(\text{vbpy})_3]^{2+}$ polymer thereby contains not only chain polymer segments but also elements of a three-dimensional matrix of metal complexes joined by bridging- $(\text{bpy})(\text{CH}_2)_4$ - (bpy) - ligands. Analogously, poly- $[\text{Ru}(\text{bpy})_2(\text{p-cinn})_2]^{2+}$ would contain bridging structures like



where the vinyl coupling reaction is depicted as "tail-to-tail" as expected from studies of hydrodimerization of radical anions of activated olefins⁵⁷. Because of the longer spacing between the perimeters of the bipyridine ligands in equation 3, and because poly- $[\text{Ru}(\text{bpy})_2(\text{p-cinn})_2]^{2+}$ should be less highly three-dimensionally cross-linked, we anticipated that the poly- $[\text{Ru}(\text{bpy})_2(\text{p-cinn})_2]^{2+}$ polymer film would be more permeable to electroactive solutes, which was borne out by the experimental results, below.

Three classes of solute behavior were observed at these films: very fast, very slow, and measureable permeation. These and their eq. 1 characteristics are outlined in Table I.

Fast Permeation Through poly-[Ru(vbpy)₃]²⁺ Film. A voltammogram in tetraalkylammonium bromide at a rotated Pt/poly-[Ru(vbpy)₃]²⁺ electrode is shown in Figure 2, Curve B. The rising part of the bromide → bromine wave has an electrochemically irreversible shape; its gently sloping wave plateau has superimposed upon it the film electrode poly-[Ru(vbpy)₃]^{3+/2+}

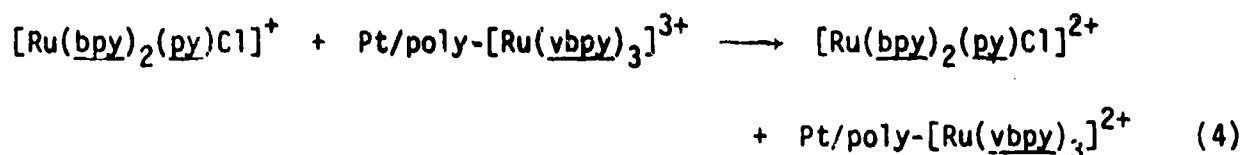
cyclic voltammogram which is shown in Curve A at the same electrode rotation rate in bromide-free solution. Limiting currents for the bromide/bromine reaction measured at +0.95 volt. vs. SSCE follow the Levich equation (Figure 2 inset, proportional to $\omega^{1/2}$, i.e., the right-hand term of eq. 1 is dominant). Further, the shape of a bromide oxidation voltammogram at a naked rotated Pt disk^{58a} is identical to Figure 2, Curve B, at all potentials more negative than +0.95 volt, and its limiting currents (at +0.95 volt) fall exactly on those in the Figure 2 inset.

These results demonstrate that bromide permeation through poly-[Ru(vbpy)₃]²⁺ to react at the Pt surface is too fast to measure at our accessible electrode rotation rates, for the film thicknesses employed, up to 3.6×10^{-9} mol./cm² or ca. 210 Å. Assuming that a 10% deviation from the Levich plot (Figure 2 inset) could have been detected at the highest electrode rotation rate, we estimate that $PD_{S,pol}/d > 0.17$, or $PD_{S,pol}C_{Ru} > 6.0 \times 10^{-10}$ for bromide permeation. Rotated electrodes coated with much thicker films of poly-[Ru(vbpy)₃]²⁺ would be necessary to further define the bromide permeability. The high bromide permeability is relevant to understanding charge transport rates through poly-[Ru(vbpy)₃]²⁺ films as further discussed below.

Very Slow Permeation Through poly-[Ru(vbpy)₃]²⁺ Film. At naked Pt, an acetonitrile solution of Ru(bpy)₂(py)Cl⁺ gives a reversible (slope 60 mV.) voltammetric wave, Figure 3, Curve A, with well-defined limiting currents which obey the Levich equation (inset, - x -). At Pt/poly-[Ru(vbpy)₃]²⁺, this complex gives a similarly formed voltammogram with superimposed poly-[Ru(vbpy)₃]^{3+/2+} electrode film reaction as shown in Figure 3, Curve B. However, in contrast to the bromide reaction, the

naked and coated electrode reactions occur at different potentials; the rising part of Figure 3, Curve B, is shifted by +140 mV relative to the naked electrode result (Curve A). The foot of the voltammogram at the polymer coated electrode at potentials where currents on the naked electrode are quite large, shows no hint of an attenuated facsimile of the naked electrode voltammogram (see enlargement, Figure 3).

These results can be interpreted in terms of very slow permeation of $[\text{Ru}(\text{bpy})_2(\text{py})\text{Cl}]^+$ into the $\text{poly-Ru}(\text{vbpy})_3^{2+}$ film so that the complex is not oxidized in significant quantity at the Pt/film interface, but is instead oxidized indirectly by Ru^{3+} sites near or at the film/solution interface:



Reaction 4 has a large driving force ($\Delta E^\circ = 375 \text{ mV.}$) and by comparison to mediation of the oxidation of other ruthenium complexes (e.g., $[\text{Ru}(\text{bpy})_3]^{2+}$) with smaller ΔE° but large electron transfer cross-reaction rates³³, can be expected to be quite fast. Limiting currents for Curve B accordingly obey the Levich equation, see Figure 3 inset - o - , showing that mass transfer of $[\text{Ru}(\text{bpy})_2(\text{py})\text{Cl}]^+$ limits the current, not the rate of Reaction 4. Additionally, $E_{1/2}$ for Curve B is considerably more negative than E_{surf}° for $\text{poly-}[\text{Ru}(\text{vbpy})_3]^{3+/2+}$, another manifestation of fast electron transfer as discussed in another paper⁵³.

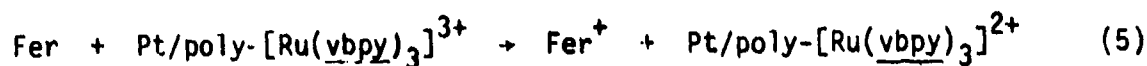
Assuming that a voltammetric wave 1% of Curve A, Figure 3, could have been detected at the foot of Curve B (but was not), we estimate that $\text{PD}_{\text{S,pol}}/d \leq 2.0 \times 10^{-4}$ or $\text{PD}_{\text{S,pol}}C_{\text{Ru}} \leq 1.6 \times 10^{-13}$ for $[\text{Ru}(\text{bpy})_2(\text{py})\text{Cl}]^+$. The same results were obtained in four experiments, where the

concentration of $[\text{Ru}(\text{bpy})_2(\text{py})\text{Cl}]^+$ was varied from 0.1 - 0.2 mM and the film coverages were 7.2, 7.8, 11.0, and 25.0×10^{-10} mol./cm² for a film thickness range of ca. 42 - 147 Å.

Measurable Permeation Rates Through poly-[Ru(vbpy)₃]²⁺. Ferrocene is oxidized in two waves at a rotated Pt/poly[Ru(vbpy)₃]²⁺ disk electrode (Figure 4, Curves A-D). The first wave ($E^{\circ'} = +0.38$ volt vs. SSCE) lies at the same potential as the naked electrode reaction (Curve E) and has limiting currents (measured at 0.6 volt) which are not proportional to $\omega^{1/2}$ (inset, -x-), but which clearly fit the membrane diffusion equation 1 by giving a linear $1/i_L$ vs. $\omega^{-1/2}$ plot (Figure 5, Curve A). Similar results were obtained in five additional experiments on electrodes with different poly-[Ru(vbpy)₃]²⁺ film thicknesses Γ_T and at different ferrocene concentrations C_S , as illustrated by the linear reciprocal Levich plots of Figure 5, Curves B and C. These data further confirm the membrane diffusion model. First, slopes of the $1/i_L$ vs. $\omega^{-1/2}$ plot are inversely proportional to C_S (compare Figure 5, Curves A vs. B) and independent of Γ_T (e.g., film thickness, compare Curves B and C). This evidence is summarized in Table II by the constancy of D_S , the diffusion coefficient for ferrocene in acetonitrile as calculated from eq. 1, and by agreement of this value with D_S observed at a rotated naked Pt electrode (2.3×10^{-5} cm²/sec.) and literature values⁵⁹. Secondly, the intercepts (Table II) of the inverse Levich plots are, within the data error limits, inversely proportional to both Γ_T and C_S , the former over nearly a ten-fold range, as shown by constancy of the intercept-derived product $PD_{S,pol}C_{Ru}$ in Table II. Thirdly, as expected from eq. 1, at sufficiently large film thicknesses (the examples with $\Gamma_T = 2.5 \times 10^{-9}$ and 6.8×10^{-9} mol./cm²),

transport through the polymer film is so slow that the limiting current for the (first) ferrocene oxidation wave becomes essentially independent of the electrode rotation rate.

The second ferrocene oxidation wave in Figure 4, Curves A-D at $E \sim +0.85$ V is due to the rapid poly-[Ru(vbpy)₃]³⁺ electron transfer mediated reaction



which occurs on the leading edge of the poly-[Ru(vbpy)₃]^{3+/2+} wave (dashed curves) in the same manner as Rxn. 4 for [Ru(bpy)₂(py)Cl]⁺ discussed above. The appearance of the second wave supports interpretation of the first wave as representing membrane diffusion as opposed to electron transfer mediation. Reaction 5 is very fast, so that diffusion of ferrocene in the solution limits the current; the limiting current measured at 1.1 volt follows the Levich equation as shown by Figure 4, (—o—). This particular experimental situation appears not to have been previously described.

Analogous experiments were conducted for the solutes *p*-benzoquinone, diquat²⁺, [Ru(bpy)₂Cl₂], and [Fe(bpy)₂(CN)₂]. The slow membrane diffusion and small limiting currents for direct oxidation of the latter two complexes diffusing through the polymer film to the Pt/film interface are illustrated by Figure 6, Curve B for [Ru(bpy)₂Cl₂]. Curve A of Figure 6 corresponds to the [Ru(bpy)₂Cl₂]^{+1/0} reaction at naked Pt (limiting currents follow the Levich relationship, Figure 6 insert —x—). Even with very thin poly-[Ru(vbpy)₃]²⁺, $\Gamma_T = 7.8 \times 10^{-10}$ mol./cm², or ca. 46 Å, the currents from Curve B are nearly independent of ω (Figure inset —●—)

and give $1/i_0$ vs. $\omega^{-1/2}$ plots according to eq. 1. Results at different C_S (constant D_S from slope) and Γ_T (constant $PD_{S,pol}C_{Ru}$ from the intercept), Table II, again support adherence to the membrane diffusion theory, eq. 1. The voltammograms and numerical data for $[Fe(bpy)_2(CN)_2]$ are similar. The data scatter in $PD_{S,pol}C_{Ru}$ is larger than that for ferrocene owing to the small slopes of the reciprocal Levich plots and to the small measured limiting currents, but general adherence to the membrane relation is obvious.

Like ferrocene, a second (rapid electron transfer mediated) wave is observed for $[Ru(bpy)_2Cl_2]$ and $[Fe(bpy)_2(CN)_2]$, the overall limiting current ($-o-$) of which is, like that at naked Pt ($-x-$), proportional to $\omega^{1/2}$ (Figure 6 inset) and controlled by diffusion of the complex in the solution.

p-benzoquinone and diquat reductions occur in two one-electron waves on naked Pt; the first wave for each is sufficiently positive of the poly- $[Ru(vbpy)_3]^{2+/1+}$ reaction that electron transfer mediation of the reduction isn't expected. The permeation wave for diquat²⁺ occurs (Figure 7, Curve B) at the same potential as diquat²⁺ reduction on naked Pt (Curve A), and gives linear reciprocal Levich plots (Figure 7 inset). D_S and $PD_{S,pol}C_{Ru}$ results for diquat²⁺, and for benzoquinone, are given in Table II.

Average $PD_{S,pol}C_{Ru}$ values in Table II display interesting and systematic variations which are discussed later.

Measurable Permeation Rates Through poly- $[Ru(bpy)_2(p-cinn)_2]^{2+}$. Voltammetry of $[Ru(bpy)_2Cl_2]$ and of ferrocene solutions at rotated poly- $[Ru(bpy)_2(p-cinn)_2]^{2+}$ disk electrodes is very similar to that in Figures 4-6, and $1/i_0$ vs. $1/\omega^{1/2}$ plots are linear with intercepts inversely propor-

tional to Γ_T . Results for $[\text{Ru}(\text{bpy})_2\text{Cl}_2]$ and ferrocene permeation into $\text{poly-}[\text{Ru}(\text{bpy})_2(\text{p-cinn})_2]^{2+}$, where C'_{Ru} is the concentration of redox sites (Table III), are both about six times larger than $\text{PD}_{\text{S,pol}}C_{\text{Ru}}$ for $[\text{Ru}(\text{bpy})_2\text{Cl}_2]$ and ferrocene in $\text{poly-}[\text{Ru}(\text{vbpy})_3]^{2+}$ (Table II). The striking permeability differences between the two solutes in each film and between the two films are illustrated in Figure 8. Expressed as $\text{PD}_{\text{S,pol}}C$, the $\text{poly-}[\text{Ru}(\text{bpy})_2(\text{p-cinn})_2]^{2+}$ film is more permeable.

Permeation Rates Through poly-Vinyldiquat²⁺. In electrochemical polymerization of the vinyldiquat monomer (VDQ^{2+}), the film thickness as with the ruthenium complex polymers, is controlled by the period of reduction, monomer concentration, and mass transfer mode, and is measured in terms of the coverage of electroactive diquat sites, $\Gamma_T \text{ mol./cm}^2$, from the charge under slow potential sweep cyclic voltammograms of the film's $\text{poly-VDQ}^{2+/+}$ reaction. The Pt/poly-VDQ^{2+} film, formed from a sterically smaller, monovinyl species, is expected to be a linear chain, polycationic polymer⁵.

Ferrocene is oxidized at a rotated Pt/poly-VDQ^{2+} disk electrode (Figure 9, Curve B) at the same potential as on naked Pt (Curve A), but with much smaller limiting current. Limiting currents (measured at +0.6 V) give linear reciprocal Levich plots the intercepts of which lead to constant $\text{PD}_{\text{S,pol}}C_{\text{VDQ}}$ values (Table IV) over a three-fold range of Γ_T . Permeation of $[\text{Ru}(\text{bpy})_2\text{Cl}_2]$ and of $[\text{Ru}(\text{bpy})_3]^{2+}$ through the same $\Gamma_T = 1.3 \times 10^{-9} \text{ mol/cm}^2$ Pt/poly-VDQ^{2+} electrode employed in the ferrocene experiments gave very small, nearly rotation rate-independent limiting currents for oxidation of the complexes; their $\text{PD}_{\text{S,pol}}C_{\text{VDQ}}$ values are lower than those for ferrocene (Table IV).

Permeabilities for ferrocene through the thinnest poly-VDQ^{2+} films are difficult to reproduce. For instance, a film specimen with coverage

$\Gamma_T \sim 2 \times 10^{-10} \text{ mol./cm}^2$ gave a much larger permeability than that in Table IV, presumably because of a high incidence of pinholes at this extreme thinness. Since a poly-VDQ²⁺ film with $\Gamma_T = 4.4 \times 10^{-10} \text{ mol./cm}^2$ corresponds (assuming unit film density or $C_{\text{VDQ}} = 2.4 \text{ M}$) to an average ca. 19 Å thickness, it is understandable that it is technically difficult to avoid pinholes. That the still very thin $\Gamma_T = 4.4 \times 10^{-10} \text{ mol./cm}^2$ film was successfully made and shows a modest permeability which is the same as that of a film three times as thick is itself rather remarkable.

Figure 9 shows also cyclic voltammetry of ferrocene at stationary naked Pt and Pt/poly-VDQ²⁺ electrodes. The classically shaped naked electrode wave (Curve C) is altered to a shape (Curve D) similar to a "CE mechanism" voltammogram⁶⁰, where the electrochemical reaction is preceded by a kinetically slow reaction. In Curve D, the slow step is the membrane diffusion process. Permeabilities could in principle be evaluated from studying Curve D as a function of potential sweep rate, but the rotated disk approach is based on a simpler theoretical formulation.

Comparison of Permeabilities. Experimental results for $\text{PD}_{\text{S,pol}}^{\text{C}}$ (Tables II - IV) are converted in Table V to $\text{PD}_{\text{S,pol}}$ based on $C_{\text{Ru}} = 1.5 \times 10^{-3}$, $C'_{\text{Ru}} = 1.3 \times 10^{-3}$, and $C_{\text{VDQ}} = 2.4 \times 10^{-3} \text{ mol./cm}^3$. Given the general insolubility and cross-linked nature (of the ruthenium polymers), the swelling errors in these redox site concentrations are probably less than 2X. Even at a presumed 2X uncertainty in the derived $\text{PD}_{\text{S,pol}}$, substantial structural effects are apparent. The Table V values appear to systematically and sensitively reflect the size and charge of the electroactive solute and the polymer membrane structure.

For poly-[Ru(vbpy)₃]²⁺ films, the PD_{S,pol} values vary over a > 10⁴ range. Molecular diameters of the neutral solutes increase and solute permeabilities, PD_{S,pol}, through the poly-[Ru(vbpy)₃]²⁺ polymer films decrease in the order: p-benzoquinone, ferrocene, [Ru(bpy)₂Cl₂], [Fe(bpy)₂(CN)₂]. The differences between [Ru(bpy)₂Cl₂], (o) and ferrocene (x) permeabilities is illustrated from the slope differences in Figure 8. Such a fine grained molecular size discrimination is not at all expected if the neutral electroactive solutes primarily diffuse to the Pt electrode through generally dispersed polymer structure imperfections (e.g., pinholes and large channels) with dimensions large compared to molecular monomers. Also, such a > 100X range of permeabilities is not consistent with reaction via an electronic conduction mechanism. The permeability ordering clearly demonstrates that transport occurs mainly through spaces in the film structure which have dimensions near those of the solutes. In this sense we agree with the description of Pearce and Bard¹⁷ of a quite different polymer, that the film can be regarded as a viscous, concentrated poly-electrolyte solution into which the electroactive solute "dissolves" and diffuses.

Films of poly-[Ru(bpy)₂(p-cinn)₂]²⁺ involve longer chains bridging adjacent ruthenium sites, should also be less highly cross-linked, and are correspondingly more permeable to neutral solute than poly-[Ru(vbpy)₃]²⁺, Figure 8.

Positive charge on the electroactive solute depresses its membrane diffusion rate through the poly-cationic films. The effect in poly-[Ru(vbpy)₃]²⁺ is ca. 10X, comparing ferrocene with diquat²⁺ and [Ru(bpy)₂Cl₂] with [Ru(bpy)₂(py)Cl]⁺. Although we have no evidential basis for separating the PD_{S,pol} product it seems reasonable to assign this difference to a less than unity partition coefficient, P. Ion association in the films is probably extensive, otherwise the electrostatic cation exclusion would yield an even larger diminution in P.

In this connection, we should note that it is already evident that small cations like Li^+ and Et_4N^+ can penetrate poly- $[\text{Ru}(\text{vbpy})_3]^{2+}$ films, observing³ that the film's ohmic resistance is lowered by increasing the external concentrations of LiClO_4 and Et_4NClO_4 supporting electrolytes.

Permeabilities in the poly- VDQ^{2+} film also follow variations in solute molecular size and charge, but the data there are much less extensive. From the ferrocene data, based on a series of Γ_T , the poly- VDQ^{2+} polymer is less permeable than poly- $[\text{Ru}(\text{vbpy})_3]^{2+}$.

The relative pinhole-freeness of the electrochemically polymerized films deserves comment, since demonstrably pinhole-free films with sub-100 Å dimensions are uncommon. We suspect that the dimensional perfection of the films is aided by current density variations during electrochemical reduction of dissolved monomer. Consider that in a film of poly- $[\text{Ru}(\text{vbpy})_3]^{2+}$ in the early stages of its formation (a short period of monomer reduction), the current density for further reduction of monomer rises at any large holes and gaps in the film since the resistance to ion flow, in the solution present in those gaps, is less than that in the film⁶¹. Polymer growth is thereby promoted at the pinhole, tending to eliminate it, e.g., a self-sealing process. This characteristic of electrochemically formed polymer films is not unique to the poly- $[\text{Ru}(\text{vbpy})_3]^{2+}$ materials, since electrode passivation during monomer oxidation⁶² is a well-known phenomenon. The poly- $[\text{Ru}(\text{vbpy})_3]^{2+}$ films differ, however, by continuing to grow following sealing of pinholes owing to their ability to transport electrochemical charge to the polymer/solution boundary⁶³, where film growth continues.

Permeability and Film Thickness. The clear proportionality of the intercepts of $1/i_q$ vs. $\omega^{-1/2}$ plots to film thickness as established by

Γ_T is an additional key element in excluding pinhole or channel phenomena in favor of the membrane diffusion model. Theory by Landsberg⁶⁴⁻⁶⁷ for reactions of solutes at active sites on rotated disks (equivalent to reactions through pinholes in a film) indicates that for the limiting condition, diffusion layer in the solution $\delta \gg$ spacing and diameter of active site, a plot of i_l^{-1} vs. $1/\omega^{1/2}$ would be linear with slope inversely proportional⁶⁸ to the overall, projected electrode area (\gg active site area) and intercept a function of the ratio of pinhole diameter and spacing. To accommodate the observed experimental behavior of the reciprocal Levich plot intercepts with this pinhole theory, the variation of the pinhole diameter/spacing ratio would have to fortuitously mimic a linear Γ_T -intercept relation. The effect would furthermore have to be reproducible over a series of electrode specimens and accurately repeated for three different polymer film structures. We believe this is a highly implausible scenario for the data in Tables II - IV. Most importantly, we draw attention again to the observed, large variations in the intercept values with solute size, as discussed above, which is inconsistent with transport through pinholes of much greater than molecular diameters.

Reciprocal Levich plot intercept- Γ_T proportionality is also important with regard to the average distance over which electrons are transferred between the Pt surface and electroactive solutes diffusing in the membrane. If the electron transfer distance were an appreciable fraction of the film thickness, then the intercept- Γ_T proportionality (at large Γ_T) would change to an exponential relation at small Γ_T , since distance-related barriers to electron transfer are exponential in form. While slight increases in $PD_{S,pol}C_{Ru}$ are observed at low Γ_T studies for several solutes in poly- $[Ru(vbpy)_3]^{2+}$, this is not generally

the case as shown in Figure 8. It is possible that fluctuations in the data at low Γ_T are due to a higher incidence of film imperfections. The thinnest films in which the Γ_T -intercept proportionality was successfully maintained are 4.1×10^{-10} mol./cm² poly-[Ru(bpy)₂(p-cinn)₂]²⁺ (ca. 34 Å based on $C_{Ru} = 1.2 \times 10^{-3}$) and 4.4×10^{-10} mol./cm² poly-VDQ²⁺ (ca. 18 Å based on $C_{VDQ} = 2.4 \times 10^{-3}$).

Thirdly, the intercept- Γ_T proportionality indicates that topological roughness (depth of valleys and mountains) of the film is not a significant fraction of film thickness for poly-[Ru(vbpy)₃]²⁺. This assertion that the microscopic roughness of the film is minimal is consistent with Γ_T -independent mediation rates $k_{crs}\Gamma$ for electron transfer reaction of the films with substrate-solutes in the solution^{33,53} where Γ is the reacting quantity of redox sites at the film/solution interface.

Finally, the measured permeabilities of $PD_{S,pol}$ in Table V can be used to estimate the average depth of permeation of an electron transfer-mediated substrate into the redox polymer film before being consumed by reaction with a mediator site. Rxn. 4 (Figure 3B) and rxn. 5 (Figure 4, second wave) are examples of such reactions. From eq. 10 in the theoretical treatment of electrocatalysis by Saveant³⁹, the ratio of permeability and mediation rates $PD_{S,pol}/k_{crs}\Gamma$ is equal to the average penetration depth. From this, penetration depths for the mediated substrates in Rxns. 4 and 5 are estimated⁶⁹ as ca. 10^{-3} and 2.6 Å, respectively. These trivially small distances support our view^{33,53} that electron transfer may actually occur without significant penetration of the substrate into the film; i.e., the redox polymer surface acts as the "electrode surface". This then is the $\kappa = 0$ case of the Saveant treatment³⁹.

Bromide Permeability and Charge Transport. The high permeability of poly-[Ru(vbpy)₃]²⁺ films to bromide ions is a significant clue in understanding charge transport through them. Charge transport through poly-[Ru(vbpy)₃]²⁺ refers to migration of electrons to/from the Pt electrode by electron self-exchange^{2,3} between neighbor redox sites, e.g.,

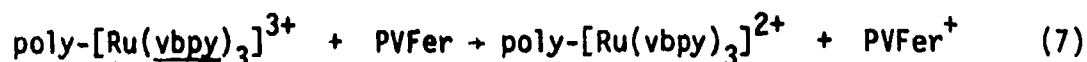


Migration of electrochemical charge in this manner is phenomenologically equivalent to diffusion and its rate can be measured⁴⁸ as a diffusion constant D_{ct} . We have measured³ D_{ct} in poly-[Ru(vbpy)₃]²⁺ films by several procedures and, assuming $C_{\text{Ru}} = 1.5 \text{ M}$, $D_{\text{ct}} = 1.8 \times 10^{-10} \text{ cm}^2/\text{sec}$.

The molecular interpretation of charge transport diffusion constants has been the object of much discussion^{22,32,39,44-52,58b} but few explicit experimental insights exist into choices between control of D_{ct} by the barrier to the electron hopping event, by the internal mobility

(self-diffusion) of redox polymer sites, or by barriers to the motion of counterions. In reaction 6, transfer of the electron must be accompanied by motion of a charge compensating perchlorate ion. If we presume (reasonably) that perchlorate and bromide ions have similar mobilities in poly-[Ru(vbpy)₃]²⁺ films, then the rate of migration of perchlorate in this film occurs (like bromide) at a rate $PD_{S,pol} > 3 \times 10^{-7} \text{ cm}^2/\text{sec}$ (Table V). This exceeds by $> 10^3 \times$ the rate of migration of electrons by reaction 6, $D_{ct} = 1.8 \times 10^{-10} \text{ cm}^2/\text{sec}$. The strong inference to be drawn from this comparison is that, for this particular redox polymer, the rate of electrochemical charge migration is not controlled by the rate of migration of ClO₄⁻ counterions, since the latter have, by analogy to bromide ions, a much higher mobility.

Redox Polymer Bilayer Films. We have recently described^{1,2} electrodes coated with two layers of redox polymers (e.g., bilayer films). The assembly Pt/poly-[Ru(vbpy)₃]²⁺/poly(vinylferrocene) is an example. The PVFer is spatially isolated from the Pt surface by the poly-[Ru(vbpy)₃]²⁺ film, forcing its oxidation reaction to occur near the electrode potential for Ru(III) production, by the mediation reaction.



which is called a (ferrocenium) charge trapping reaction.

The trapped PVFer⁺ state is stable for considerable periods when the poly-Ru(vbpy)₃²⁺ inner film layer is reasonably thick. We were interested in how thin the inner film thickness could be, yet still effect the charge trapping reaction (7) at all (as opposed to direct oxidation of PVFer by the Pt electrode), and how rapidly PVFer⁺ trapped states formed with very thin inner films leak away. Figure 10 shows a cyclic voltammogram where Γ_T for the inner film poly-Ru(vbpy)₃²⁺ layer

was only 6×10^{-10} mol./cm², or ca. 40 Å. The initial positive potential scan shows only a small anodic current inflection at ca. +0.44 volt vs. SSCE (the thermodynamic potential for PVFer oxidation in acetonitrile), and then a large current peak at +0.93 volt (Curve E) from previous studies we know to be the trapping reaction^{1,2}. This result demonstrating charge trapping for very thin inner layers, is significant in that switching times for these film assemblies as charge rectifying or as stably switched electrochromic surfaces⁵ are thereby predicted for equally thin outer films to be as short as (by the approximate thickness relation, $\sqrt{D_{ct}t}$) ca. 1 msec.

Following scanning through the poly-[Ru(vbpy)₃]^{3+/2+} wave at +1.1 volt, no reverse wave for PVFer⁺ reduction is seen (as expected^{1,2}). If the potential is scanned again positively from zero volts immediately or after pause-waiting periods of 1, 2 or 4 minutes (Curves A-D), a retrapping peak is observed near +0.9 volts whose magnitude does not increase proportionately to the waiting time. This indicates that leakage does occur for this thin inner film but not all regions of the film leak away charge at equal rates.

The wave at ca. +0.44 volt in Figure 11 is notable both for its small size and its shape. The charge under the +0.44 volt wave is < 5% of the +0.93 volt initial charge trapping peak; very little ferrocene is oxidized by permeation through the inner film poly-[Ru(vbpy)₃]²⁺ film. That which is oxidized gives a membrane diffusion cyclic voltammetric shape reminiscent of that in Figure 9, Curve D, which implies that slow diffusion of PVFer chains into the poly-Ru(vbpy)₃²⁺ polymer can occur on a time scale of a second or so. However, this polymer/polymer interpenetration does not over the course of time homogenize the films (else no trapping peak at all), so the PVFer diffusion must more resemble a large-scale polymer segment vibration than a net

diffusional mass transport. This particular observation is of interest with respect to the stability of bilayer polymer film assemblies and the kinetics of electron transfer trapping reactions at the polymer/polymer, poly-[Ru(vbpy)₃]³⁺/PVFer interface⁷⁰.

CONCLUSIONS

This paper demonstrates the feasibility of electrochemically preparing ultrathin redox polymer films which exhibit both molecular size and charge discrimination toward solutes in contact with them. This observation is significant in that the ruthenium polymers have redox properties making them potential oxidation catalysts for electro-organic reactions; their permeability characteristics also suggest the possibility of size selective oxidation processes by the polymer, and/or by the underlying electrode or other catalyst. The discrimination of molecular size is, crudely, comparable to that of zeolitic structures^{10,11}.

Acknowledgement. This research was supported in part by grants from the National Science Foundation and the Office of Naval Research.

References

1. Abruña, H. D.; Denisevich, P.; Umaña, M.; Meyer, T. J.; and Murray, R. W. J. Amer. Chem. Soc. **103** (1981) 1.
2. Denisevich, P.; Willman, K. W.; and Murray, R. W. J. Amer. Chem. Soc. **103** (1981) 4727.
3. Denisevich, P.; Abruña, H. D.; Leidner, C. R.; Meyer, T. J.; and Murray, R. W. Inorg. Chem., in press.
4. Schmehl, R.; and Murray, R. W., unpublished results.
5. Willman, K. W.; and Murray, J. Electroanal. Chem., in press.
6. Blank, M., Ed.; "Biochemistry: Ions, Surfaces, Membranes", Adv. Chem. Series, vol. 88, 1980.
7. Tepfer, M.; and Taylor, I. E. P. Science **213** (1981) 761.
8. Kydonieus, A. F. "Controlled Release Technologies: Methods, Theory, and Applications", vol. 1, CRC Press, 1980, pp.
9. Carr, R. W.; and Bowers, L. D. "Immobilized Enzymes In Analytical and Clinical Chemistry", John Wiley and Sons, New York, 1980.
10. Barrer, R. M. "Molecular Sieve Zeolite", Adv. Chem. Series, **102** (1971) 41.
11. Eberly, P. E. "Zeolite Chemistry and Catalysis", Rabo, J. A.; ACS Monograph Series, ACS Press, 1976, pp. 392.
12. Fendler, J. H.; and Fendler, E. J. "Catalysis in Micellar and Macromolecular Systems", Academic Press, New York, 1975.
13. Infelta, P. P.; Gratzel, M.; and Fendler, J. H. J. Amer. Chem. Soc. **102** (1980) 1479.
14. Nomura, T.; Escabi-Perez, J. R.; Sunamoto, J.; and Fendler, J. H. J. Amer. Chem. Soc. **102** (1980) 1484.

15. Oyama, N.; and Anson, F. C. Anal. Chem. **52** (1980) 1192.
16. Oyama, N.; Shigehara, K.; and Anson, F. C. Inorg. Chem. **20** (1981) 518.
17. Peerce, P. J.; and Bard, A. J. J. Electroanal. Chem. **112** (1980) 97.
18. Doblhofer, K.; Nolte, D.; and Ulstrup, J. Ber. Bunsenges. Phys. Chem. **82** (1978) 403.
19. Lacaze, P.-C.; Pham, M.-C.; Delamar, M.; and Dubois, J.-E. J. Electroanal. Chem. **108** (1980) 9.
20. Dautartas, M. F.; and Evans, J. F. J. Electroanal. Chem. **109** (1980) 301.
21. Schroeder, A. H.; and Kaufman, F. R. J. Electroanal. Chem. **113** (1980) 209.
22. Kaufman, F. B.; Schroeder, A. H.; Engler, E. M.; Kramer, S. R.; and Chambers, J. Q. J. Amer. Chem. Soc. **102** (1980) 483.
23. Bettelheim, A.; Chan, R. J. H.; and Kuwana, T. J. Electroanal. Chem. **110** (1980) 93.
24. DeGrand, C.; and Laviron, E. J. Electroanal. Chem. **117** (1981) 283.
25. Oyama, N.; Sato, K.; and Matsuda, H. J. Electroanal. Chem. **115** (1980) 149.
26. Samuels, G. J.; and Meyer, T. J. J. Amer. Chem. Soc. **103** (1981) 307.
27. Miller, L. L.; and Van De Mark, M. R. J. Amer. Chem. Soc. **100** (1978) 3223.
28. Miller, L. L.; and Van De Mark, M. R. J. Electroanal. Chem. **88** (1978) 437.
29. Kerr, J. B.; and Miller, L. L. J. Electroanal. Chem. **101** (1979) 263.
30. Kerr, J. B.; Miller, L. L.; and Van De Mark, M. R. J. Amer. Chem. Soc. **102** (1980) 3383.
31. DeGrand, C.; and Miller, L. L. J. Electroanal. Chem. **117** (1981) 267.
32. Kuo, K. N.; and Murray, R. W. J. Electroanal. Chem., in press.
33. Ikeda, T.; Leidner, C. R.; and Murray, R. W. J. Amer. Chem. Soc., in press.
34. Rocklin, R. D.; and Murray, R. W. J. Phys. Chem. **85** (1981) 2104.
35. Murray, R. W. Philosoph. Trans. Royal Society, London, Phil. Trans. R. Soc. Lond. A **302** (1981) 253.

36. Andrieux, C. P.; and Saveant, J.-M. J. Electroanal. Chem. **93** (1978) 163.
37. Andrieux, C. P.; Dumas-Bouchiat, J. M.; and Saveant, J.-M. J. Electroanal. Chem. **114** (1980) 159.
38. Andrieux, C. P.; and Saveant, J.-M. J. Electroanal. Chem. **111** (1980) 377.
39. Andrieux, C. P.; Dumas-Bouchiat, J. M.; and Saveant, J.-M., J. Electroanal. Chem., in press.
40. Bolts, J. M.; Bocarsly, A. B.; Palazzotto, M. C.; Walton, E. G.; Lewis, N. S.; and Wrighton, M. S. J. Amer. Chem. Soc. **101** (1979) 1378.
41. Bookbinder, D. C.; Lewis, N. S.; Bradley, M. G.; Bocarsly, A. B.; and Wrighton, M. S. J. Amer. Chem. Soc. **101** (1979) 7721.
42. Lewis, N. S.; Bocarsly, A. B.; and Wrighton, J. Phys. Chem. **84** (1980) 2033.
43. Dautartas, M. F.; Mann, K. R.; and Evans, J. F. J. Electroanal. Chem. **110** (1980) 379.
44. Anson, F. C. J. Phys. Chem. **84** (1980) 3336.
45. Peerce, P. J.; and Bard, A. J. J. Electroanal. Chem. **114** (1980) 89.
46. Schroeder, A. H.; Kaufman, F. B.; Patel, V.; and Engler, E. M. J. Electroanal. Chem. **113** (1980) 193.
47. Laviron, E. J. Electroanal. Chem. **112** (1980) 1.
48. Daum, P.; Lenhard, J. R.; Rolison, D. R.; and Murray, R. W. J. Amer. Chem. Soc. **102** (1980) 4649.
49. Nowak, R. J.; Schultz, F. A.; Umaña, M.; Lam, R.; and Murray, R. W. Anal. Chem. **52** (1980) 315.
50. Daum, P.; and Murray, R. W. J. Electroanal. Chem. **103** (1979) 289.
51. Daum, P.; and Murray, R. W. J. Phys. Chem. **85** (1981) 389.
52. Facci, J.; and Murray, R. W. J. Electroanal. Chem., **124** (1981) 339.
53. Ikeda, T.; Leidner, C. R.; and Murray, R. W., submitted.
54. Sullivan, B. P.; Salmon, D. J.; and Meyer, T. J. Inorg. Chem. **17** (1978) 3334.

55. Schilt, A. A. Inorg. Synth. 12 (1970) 247.
56. Gough, D. A.; and Leyboldt, J. K. Anal. Chem. 51 (1979) 439.
57. Bazier, M. M.; "Organic Electrochemistry", M. M. Bazier, ed., New York, Marcel Dekker, 1973, pp. 679-704.
58. a) Rubenstein, I.; J. Phys. Chem. 85 (1981) 1899;
b) Rubenstein, I.; and Bard, A. J. J. Amer. Chem. Soc. 103 (1981) 5007.
59. Kuwana, T.; Bublitz, D. E.; and Hom, G. J. Amer. Chem. Soc. 82 (1960) 5811.
60. Nicholson, R. S.; and Shain, I.; Anal. Chem. 36 (1964) 706.
61. That current density uniformity is important is shown by considerable sensitivity to the placement of the auxiliary electrode during polymerization³.
62. Baizer, M. M.; "Organic Electrochemistry", M. M. Bazier, ed., New York, Marcel Dekker, 1973, pp. 947-975.
63. Including the boundary of the inner surface of any remaining gaps or canyons.
64. Gueshi, T.; Tokuda, K.; and Matsuda, H. J. Electroanal. Chem. 89 (1978) 247.
65. Landsberg, R.; and Thiele, R. Electrochim. Acta 11 (1966) 1243.
66. Scheller, F.; Muller, S.; Landsberg, R.; and Spitzer, H.-J. J. Electroanal. Chem. 19 (1968) 187.
67. Scheller, F.; Landsberg, R.; and Muller, S. J. Electroanal. Chem. 20 (1969) 375.
68. We observe this, since D_S determined from the reciprocal Levich plots agrees with naked electrode D_S .
69. The Levich behavior in Figure 4 (—o—) for the mediated ferrocene oxidation rxn. 5 indicates that $k_{crs} \Gamma > \sim 0.5$ cm/s., i.e., is beyond our measurable⁵³ limit. With the measured $PD_{S, pol} = 1.3 \times 10^{-8}$ cm²/s. for ferrocene in Table V, the estimation of ferrocene penetration beyond the

poly-[Ru(vbpy)₃]²⁺/solution interface is simply, $\rho_{S,pol}/k_{crs} \Gamma > 2.6 \times 10^{-8}$ cm., less than a monolayer dimension. The calculation for Rxn. 4 is done similarly.

70. Denisevich, P.; Willman, K.; and Murray, R. W., unpublished results.

TABLE I

CLASSES OF BEHAVIOR OBSERVED FOR SOLUTE PERMEATION THROUGH $\text{poly}[\text{Ru}(\text{vbpy})_3]^{2+}$ POLYMER FILMS

<u>Rate of Solute (Reactant) Permeation</u>	<u>Reaction Site(s)</u>	<u>Waves Observed</u>	<u>Potential of solute reaction; diagnostic characteristics</u>	<u>Examples</u>
very fast	Electrode Surface	1	Same as at naked electrode; linear Levich plot	Br^-/Br_2
very slow	Film/solution interface	1	Shifted toward polymer potential; linear Levich plot	$[\text{Ru}(\text{bpy})_2(\text{py})\text{Cl}]^{+1/+2}$
measurable	1. Electrode surface, and 2. Film/solution interface	2	1. Same as at naked electrode; linear <u>reciprocal</u> Levich plot 2. Shifted toward polymer potential; linear Levich plot	Fer/Fer^+

TABLE II

Permeation Rates of Various Electroactive Solutes Through

Pt/poly-Ru(vbpy)₃²⁺ Films, in 0.1 M Et₄NClO₄/CH₃CN

	$\Gamma_T, \text{mol./cm}^2$	$C_S, \times 10^3 \text{ M}$	Intercept, $\times 10^{-6}, \text{ amp}^{-1}$	$D_S, \times 10^5, \text{ cm}^2/\text{s.}$	$PD_S, \text{ pol/d, cm/s.}$	$PD_S, \text{ pol } C_{Ru}, \text{ mol./cm.s.}$
Ferrocene						
$E^\circ = +0.38\text{V}$	7.2×10^{-10}	0.07	0.034	2.4	4.2×10^{-2}	3.0×10^{-11}
	7.8×10^{-10}	0.18	0.021	2.4	2.2×10^{-2}	1.7×10^{-11}
	1.1×10^{-9}	0.18	0.029	2.0	1.6×10^{-2}	1.7×10^{-11}
	1.2×10^{-9}	0.17	0.024	2.4	2.0×10^{-2}	2.4×10^{-11}
	2.5×10^{-9}	0.07	0.30 ^a	-	4.6×10^{-3}	1.2×10^{-11}
	6.8×10^{-9}	0.07	0.67 ^a	-	1.8×10^{-3}	1.2×10^{-11}
						$1.9 \pm 0.7 \times 10^{-11}$
Benzoquinone						
$E^\circ = -0.51_5\text{V}$	7.8×10^{-10}	0.12	0.0048	2.6	1.5×10^{-1}	1.2×10^{-10}
	1.1×10^{-9}	0.12	0.0080	2.2	8.9×10^{-2}	9.8×10^{-11}
	2.0×10^{-9}	0.11	0.026	4.4	2.9×10^{-2}	5.8×10^{-11}
	3.6×10^{-9}	0.11	0.035	5.0	2.1×10^{-2}	7.6×10^{-11}
						$8.7 \pm 2.1 \times 10^{-11}$
diquat²⁺						
$E^\circ = -0.37\text{V}$	7.8×10^{-10}	0.19	0.078	1.2	5.6×10^{-3}	4.4×10^{-12}
	1.1×10^{-9}	0.19	0.31	1.0	1.4×10^{-3}	1.5×10^{-12}
					D_S (at naked Pt): $1.1 \times 10^{-5} \text{ cm}^2\text{s}^{-1}$	$3.0 \pm 1.5 \times 10^{-12}$

Table II continued
page 2 of 2

$\text{Ru}(\text{bpy})_2\text{Cl}_2$

E°	7.8×10^{-10}	0.17	0.35	1.4	1.4×10^{-3}	1.1×10^{-12}
$+0.29_5 \text{ V}$	9.7×10^{-10}	0.04	0.82	1.1	2.5×10^{-3}	2.4×10^{-12}
	9.7×10^{-10}	0.09	0.29	0.81	3.2×10^{-3}	3.1×10^{-12}
	9.7×10^{-10}	0.15	0.19	0.84	3.0×10^{-3}	2.9×10^{-12}
	1.1×10^{-9}	0.17	0.62	0.84	7.8×10^{-4}	8.6×10^{-13}
	1.2×10^{-9}	0.12	0.33 ^a	-	2.1×10^{-3}	2.5×10^{-12}
	2.1×10^{-9}	0.12	1.33 ^a	-	5.2×10^{-4}	1.0×10^{-12}
D_S (at naked Pt): $1.3 \times 10^{-5} \text{ cm}^2 \text{ s}^{-1}$						
$2.0 \pm 0.9 \times 10^{-12}$						

$\text{Fe}(\text{bpy})_2(\text{CN})_2$

$E^\circ = +0.44_5 \text{ V}$	7.8×10^{-10}	0.18	0.83 ^a	-	5.5×10^{-4}	4.3×10^{-13}
	1.2×10^{-9}	0.14	1.0 ^a	-	5.9×10^{-4}	7.1×10^{-13}
	2.7×10^{-9}	0.32	2.0 ^a	-	1.3×10^{-4}	3.5×10^{-13}
D_S (at naked Pt): $0.87 \times 10^{-5} \text{ cm}^2 \text{ s}^{-1}$						
						$5.0 \pm 2.0 \times 10^{-13}$

a. $i_g \neq f(\omega^{1/2})$

b. $D_S = 2.4 \times 10^{-5} \text{ cm}^2 \text{ s}^{-1}$ from ref. 59, $2.8 \times 10^{-5} \text{ cm}^2 \text{ s}^{-1}$ from ref. 5-9.

TABLE III

Permeation Rates of Electroactive Solutes Through
Pt/poly-[Ru(bpy)₂(p-cinn)₂]²⁺ Films in 0.1 M Et₄NCIO₄/CH₃CN

	$\Gamma_T, \text{mol./cm}^2, \times 10^{10}$	$C_S, \times 10^3, \text{M}$	$D_S \times 10^5, \text{cm}^2 \text{sec}^{-1}$	$PD_{S, \text{pol}} C'_{\text{Ru}}, \text{mol./cm.s.}$
[Ru(bpy) ₂ Cl ₂]	4.11	0.0826	1.65	1.2×10^{-11}
	7.83	0.0826	1.51	1.5×10^{-11}
	9.68	0.0826	1.88	9.2×10^{-12}
	11.9	0.067	1.85	1.1×10^{-11}
	21.2	0.0826	-	1.7×10^{-11}
	25.0	0.10	0.45	1.5×10^{-11}
	49.6	0.067	0.99	1.4×10^{-11}
	49.6	0.10	1.05	1.1×10^{-11}
	130.0	0.10	-	1.5×10^{-11}
				Avg. $1.3_5 \times 10^{-11}$
ferrocene	15.2	0.135	2.11	12.6×10^{-11}
	23.4	0.10	1.25	8.8×10^{-11}
	28.1	0.135	1.90	17.1×10^{-11}
	46.6	0.135	2.02	13.5×10^{-11}
	55.3	0.135	1.89	11.7×10^{-11}
	58.1	0.10	1.22	8.3×10^{-11}
	75.7	0.10	1.41	10.6×10^{-11}
				Avg. 11.8×10^{-11}

TABLE IV

Permeation Rates of Electroactive Solutes Through
Pt/poly-VDQ²⁺ Films in 0.1 M Et₄NClO₄/CH₃CN

	$\Gamma_T, \text{mol./cm}^2$	$C_S, \times 10^3 \text{ M}$	Intercept, $\times 10^{-6}, \text{ amp}^{-1}$	$D_S \times 10^5, \text{ cm}^2/\text{s}$	$PD_S, \text{ pol/d, cm}^2 \text{ s}^{-1}$	$PD_S, \text{ pol}^C \text{ VDQ}^{\text{mol}} \text{ s}^{-1} / \text{cm}.$
Ferrocene	4.4×10^{-10}	0.10	0.16	2.7	5.1×10^{-3}	2.2×10^{-12}
	6.3×10^{-10}	0.10	0.23	1.2	3.5×10^{-3}	2.2×10^{-12}
	1.3×10^{-9}	0.18	0.27	1.8	2.2×10^{-3}	2.9×10^{-12}
$[\text{Ru}(\text{bpy})_2\text{Cl}_2]$	1.3×10^{-9}	0.26	0.68 ^a	-	6.1×10^{-4}	7.9×10^{-13}
$[\text{Ru}(\text{bpy})_3]^{2+}$	1.3×10^{-9}	0.15	2.7 ^a	-	2.7×10^{-4}	3.5×10^{-13}

a. $i_1 \neq f(\omega^{1/2})$

TABLE V

PD_{S,pol} For Various Electroactive Solutes
Through Electrochemically Polymerized Films^a

Solute	PD _{S,pol} through: poly-[Ru(vbpy) ₃] ²⁺ ^b	poly-[Ru(bpy) ₂ (p-cinn) ₂] ²⁺ ^c	poly-VDQ ²⁺ ^d
bromide	$> 4 \times 10^{-7}$		
p-benzoquinone	5.8×10^{-8}		
ferrocene	1.3×10^{-8}	9.0×10^{-8}	1.0×10^{-9}
[Ru(bpy) ₂ Cl ₂]	1.3×10^{-9}	1.0×10^{-8}	3.3×10^{-10}
[Fe(bpy) ₂ (CN) ₂]	3.3×10^{-10}		
diquat ²⁺	2.0×10^{-9}		
[Ru(bpy) ₂ (py)Cl] ⁺	$< 7 \times 10^{-12}$		
[Ru(bpy) ₃] ²⁺			1.5×10^{-10}

a. Assuming maximum redox site concentrations as in footnotes b, c, d, for unswollen films.

b. $C_{Ru} = 1.5 \times 10^{-3}$ mol./cm³ based on 1.35 g./cm³ density³.

c. $C_{Ru} = 1.3 \times 10^{-3}$ mol./cm³ based on 1.40 g./cm² density.

d. $C_{VDQ} = 2.4 \times 10^{-3}$ mol./cm³ based on assumed unity density.

FIGURE LEGENDS

Figure 1. Cyclic voltammetry at 0.1 v/s of $\text{Ru}^{\text{III/II}}$ reaction for $\text{Pt/poly-}[\text{Ru}(\text{vbpy})_3]^{2+}$ (Curve A) and $\text{Pt/poly-}[\text{Ru}(\text{bpy})_2(\text{p-cinn})_2]^{2+}$ (Curve B) electrodes in 0.1 M $\text{Et}_4\text{NClO}_4/\text{CH}_3\text{CN}$. $\Gamma_T = 5.8 \times 10^{-9}$ and $5.3 \times 10^{-9} \text{ mol./cm}^2$, respectively.

Figure 2. Rotated $\text{Pt/poly-}[\text{Ru}(\text{vbpy})_3]^{2+}$ ($\Gamma_T = 3.6 \times 10^{-9} \text{ mol./cm}^2$) disk voltammetry in 0.1 M $\text{Et}_4\text{NClO}_4/\text{CH}_3\text{CN}$. No added bromide (Curve A); 0.1- mM Bu_4NBr (Curve B). $v = 0.02 \text{ v/s}$, $S = 77 \mu\text{A/cm}^2$, $\omega = 6400 \text{ rpm}$. Inset is limiting current measured at 0.95 v. as a function of $\omega^{1/2}$.

Figure 3. Rotated disk voltammograms of 0.20 mM $[\text{Ru}(\text{bpy})_2(\text{py})\text{Cl}]^+$ in 0.1 M $\text{Et}_4\text{NClO}_4/\text{CH}_3\text{CN}$ at naked Pt (Curve A) and $\text{Pt/poly}[\text{Ru}(\text{vbpy})_3]^{2+}$ ($\Gamma_T = 7.8 \times 10^{-10} \text{ mol./cm}^2$) (Curve B) electrodes. $v = 0.02 \text{ v/s}$, $S = 77 \mu\text{A/cm}^2$, $\omega = 6400 \text{ rpm}$. Figure insets are Levich plots of limiting currents of Curve A (—x—) and Curve B (—o—) and 10X scale expansion ($S = 7.7 \mu\text{A/cm}^2$) of foot of Curve B.

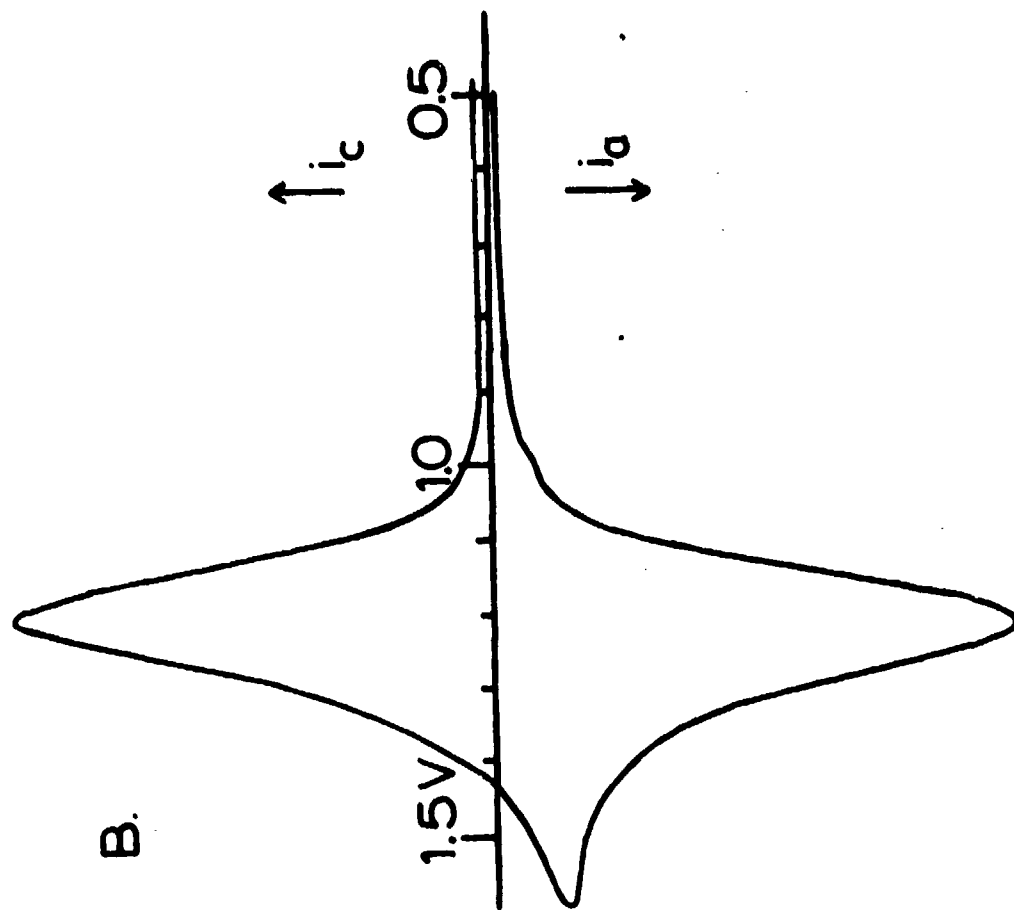
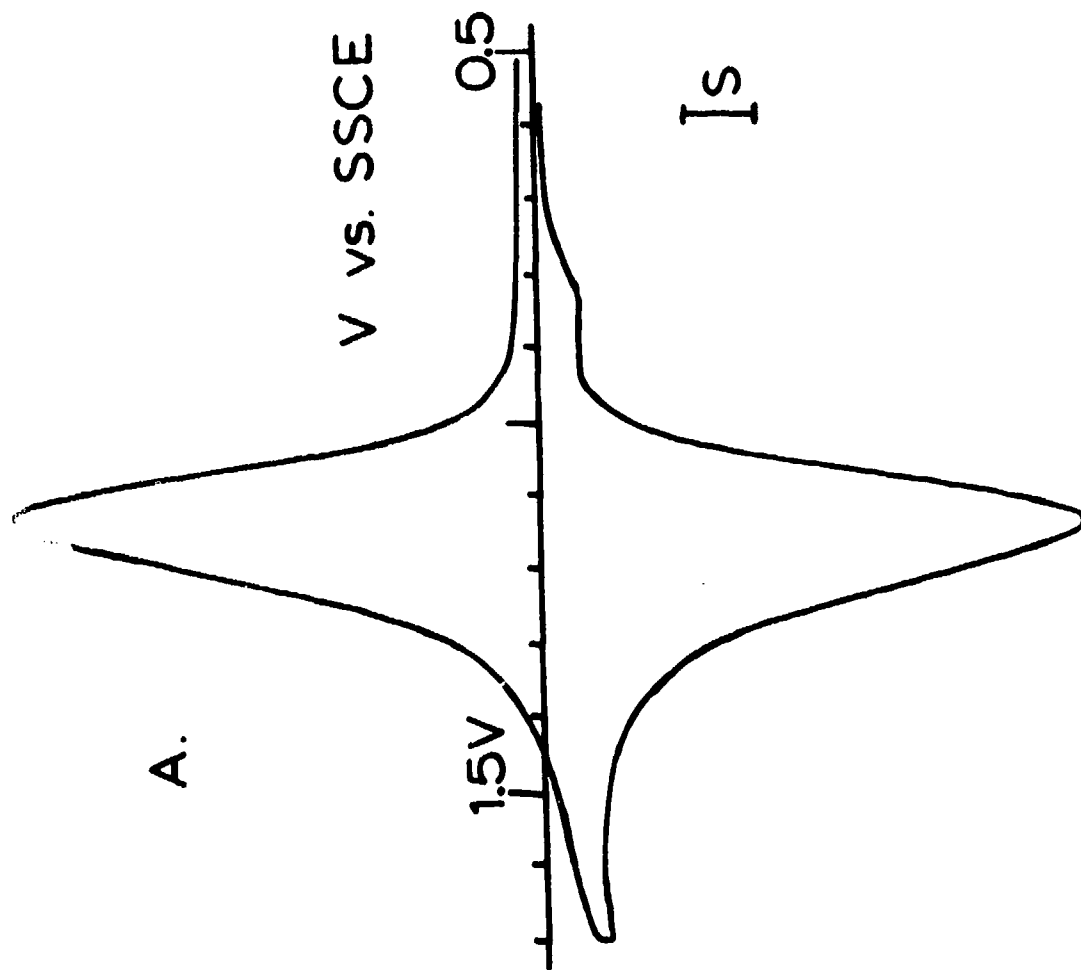
Figure 4. Rotated disk voltammograms of 0.070 mM ferrocene in 0.1 M $\text{Et}_4\text{NClO}_4/\text{CH}_3\text{CN}$ at $\text{Pt/poly-Ru}(\text{vbpy})_3^{2+}$ ($\Gamma_T = 7.2 \times 10^{-10} \text{ mol./cm}^2$) (Curves A - D, electrode rotation rate 400, 1600, 3600, and 6400 rpm, respectively), and naked Pt (Curve E, 6400 rpm). $v = 0.02 \text{ v/s}$, $S = 19 \mu\text{A/cm}^2$. Figure inset is limiting currents of ferrocene at naked Pt (—●—) and at $\text{Pt/poly-Ru}(\text{vbpy})_3^{2+}$ for permeation wave (—x—) measured at 0.6 volt and mediated wave (—o—) measured at 1.1 volt.

- Figure 5. Reciprocal Levich plots for permeation wave for ferrocene oxidation at Pt/poly-Ru(vbpy)₃²⁺. Curve A - C: C_S = 0.070, 0.18, 0.18 mM; $\Gamma_T = 7.2 \times 10^{-10}$, 1.1×10^{-9} , 7.8×10^{-10} mol./cm², respectively.
- Figure 6. Rotated disk voltammogram at 0.17 mM [Ru(bpy)₂Cl₂] in 0.1 M Et₄NCIO₄/CH₃CN at naked Pt (Curve A) and (Curve B) Pt/poly-[Ru(vbpy)₃]²⁺ ($\Gamma_T = 7.8 \times 10^{-10}$ mol./cm²) electrodes. $v = 0.02$ v/s, $S = 77 \mu\text{a/cm}^2$, $\omega = 6400$ rpm. Inset is limiting currents measured at (—x—) 0.5 volt on Curve A and at (—●—) 0.5 volt and (—o—) 1.1 volt on Curve B.
- Figure 7. Rotated disk voltammograms of 0.19 mM diquat²⁺ in 0.1 M Et₄NCIO₄/CH₃CN at naked Pt (Curve A) and Pt/poly-[Ru(vbpy)₃]²⁺ ($\Gamma_T = 7.8 \times 10^{-10}$ mol./cm²) electrodes. $v = 0.02$ v/s, $S = 39 \mu\text{a/cm}^2$, $\omega = 6400$ rpm. Figure inset is reciprocal Levich plot for limiting currents of Curve B (Line 1) and of another example where $\Gamma_T = 1.1 \times 10^{-9}$ mol./cm² (Line 2).
- Figure 8. PD_S/d from reciprocal Levich plot intercepts are inversely proportional to Γ_T , film thickness. Results for ferrocene (x) and [Ru(bpy)₂Cl₂] (o) in poly-[Ru(vbpy)₃]²⁺ (— — —) and for ferrocene (●) and [Ru(bpy)₂Cl₂] (Δ) in poly-[Ru(bpy)₂(p-cinn)₂]²⁺ (— — —).
- Figure 9. Rotated disk voltammetry of 0.1 mM ferrocene in 0.1 M Et₄NCIO₄/CH₃CN at naked Pt (Curve A) and Pt/poly-VDQ²⁺ ($\Gamma_T = 6.3 \times 10^{-10}$ mol./cm²). $v = 0.02$ v/s, $S = 19 \mu\text{a/cm}^2$, $\omega = 3600$ rpm. Stationary electrode cyclic voltammetry for naked Pt (Curve C) and Pt/poly-VDQ²⁺ (Curve D)

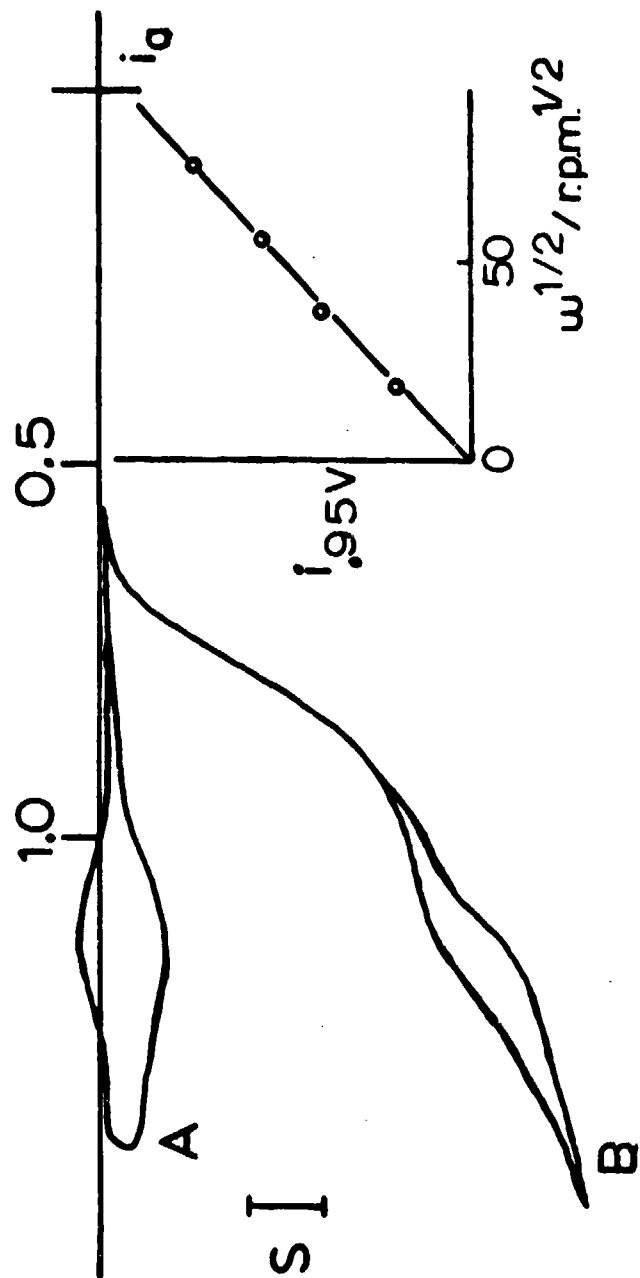
Figure 9 continued:

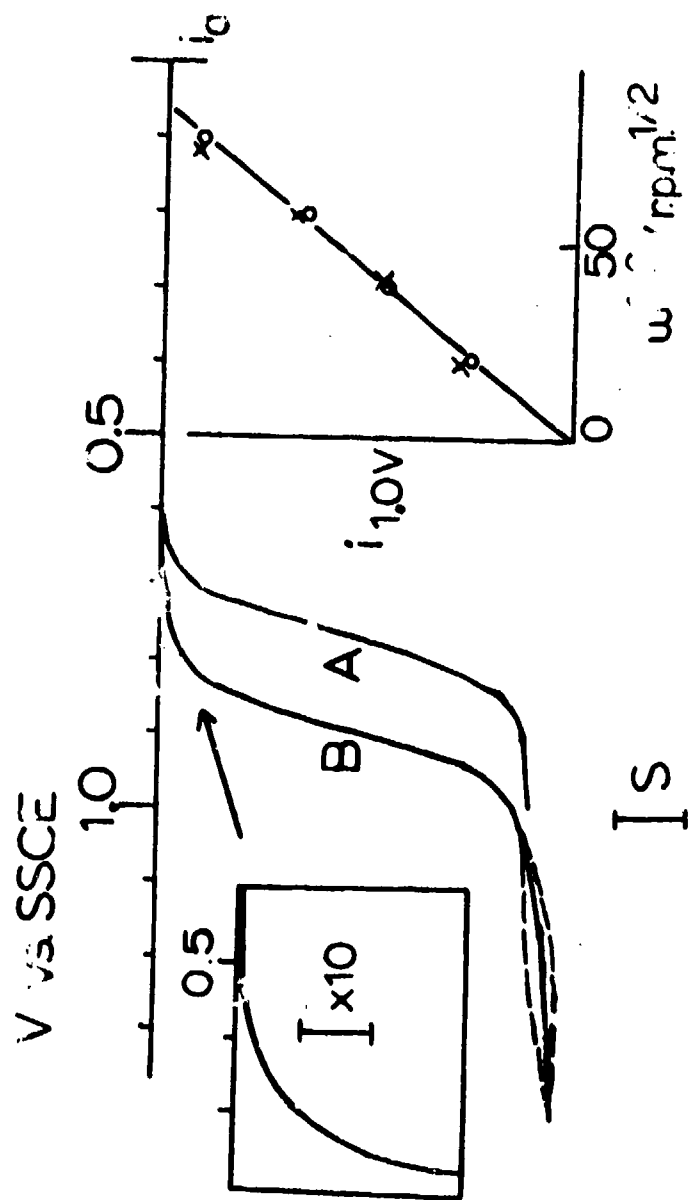
in same solution at 0.1 v/s.

Figure 10. Cyclic voltammetry (0.1 v/s) of a Pt/poly-Ru(vbpy)₃]²⁺/PVFer bilayer electrode were Γ_{inner} is 6×10^{-10} mol./cm². Curve E: virgin scan 0 → +1.6 → 0 volt; Curve A: immediately repeated scan; Curves B - D repeated after 1, 2, 4 minute pause at 0 volt, respectively. Charges under trapping peaks are (Curves A - E), 1.6×10^{-10} , 3.8×10^{-10} , 6.2×10^{-10} , 8.9×10^{-10} , 2.5×10^{-9} mol./cm².



V vs. SSCE





V vs. SSCE

1.0
0.5

i_d

A

B

C

D

I_s

E

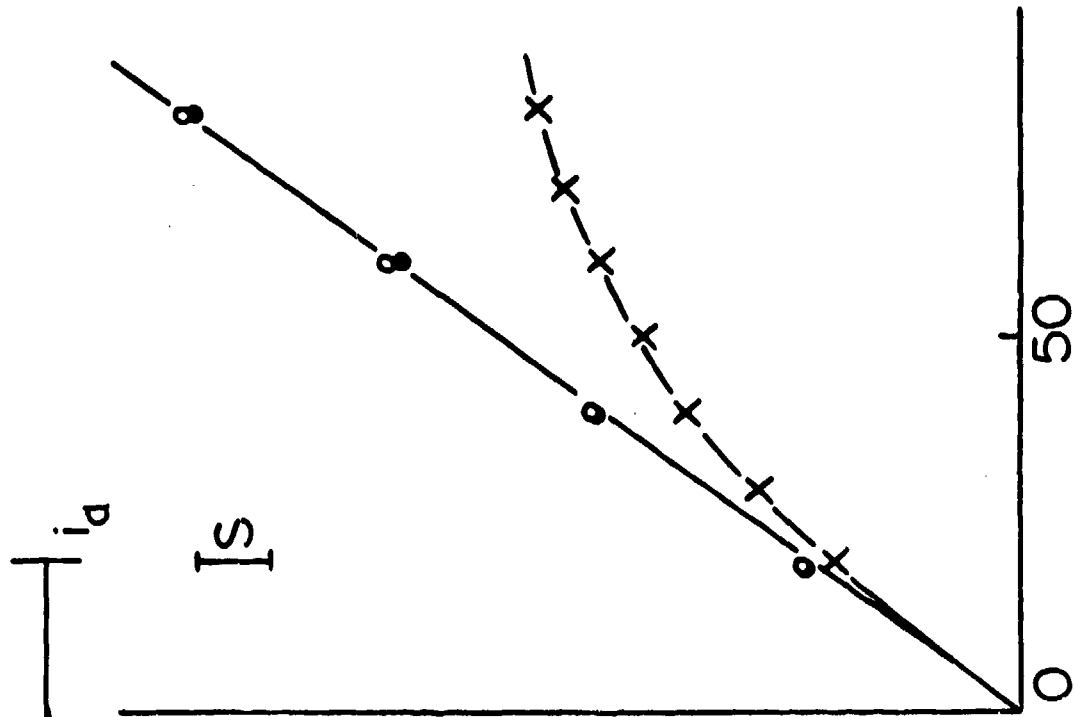
i_a

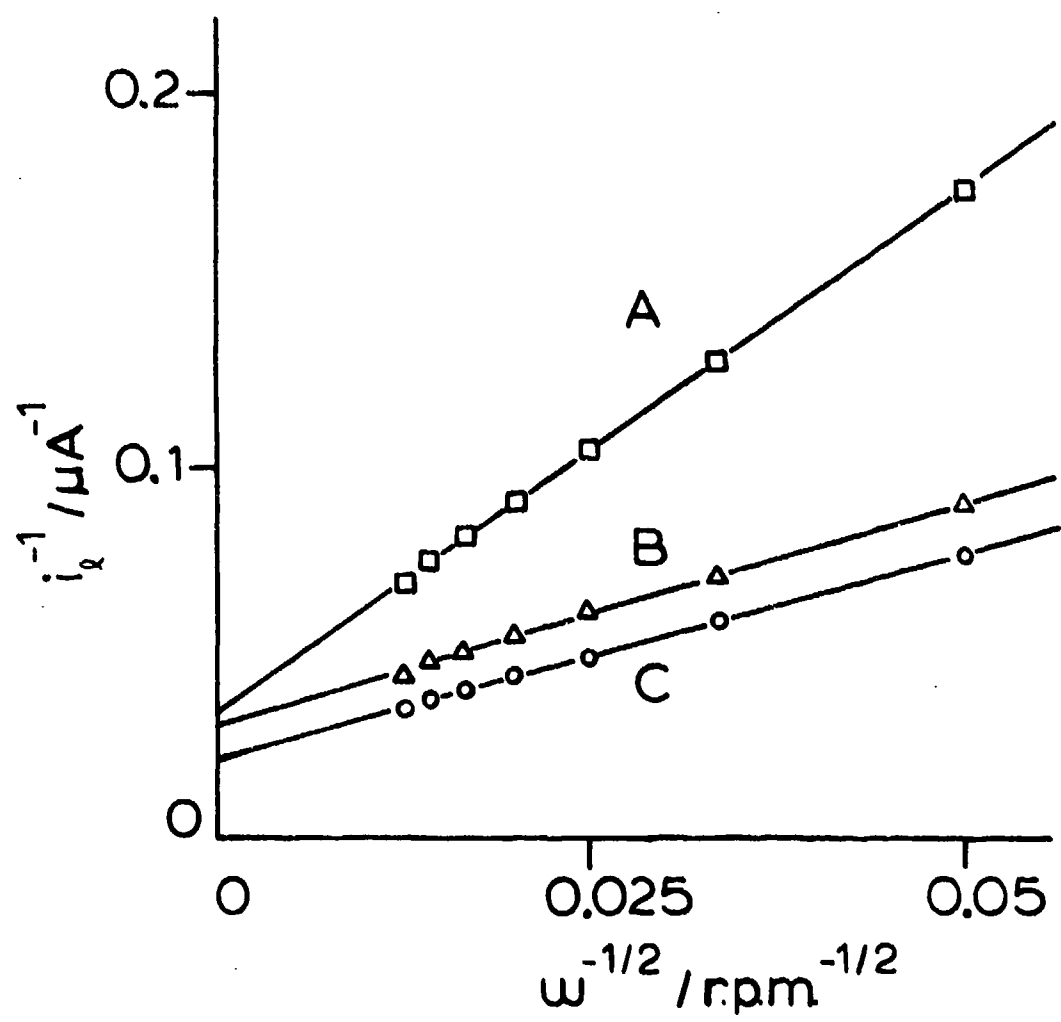
I_s

O

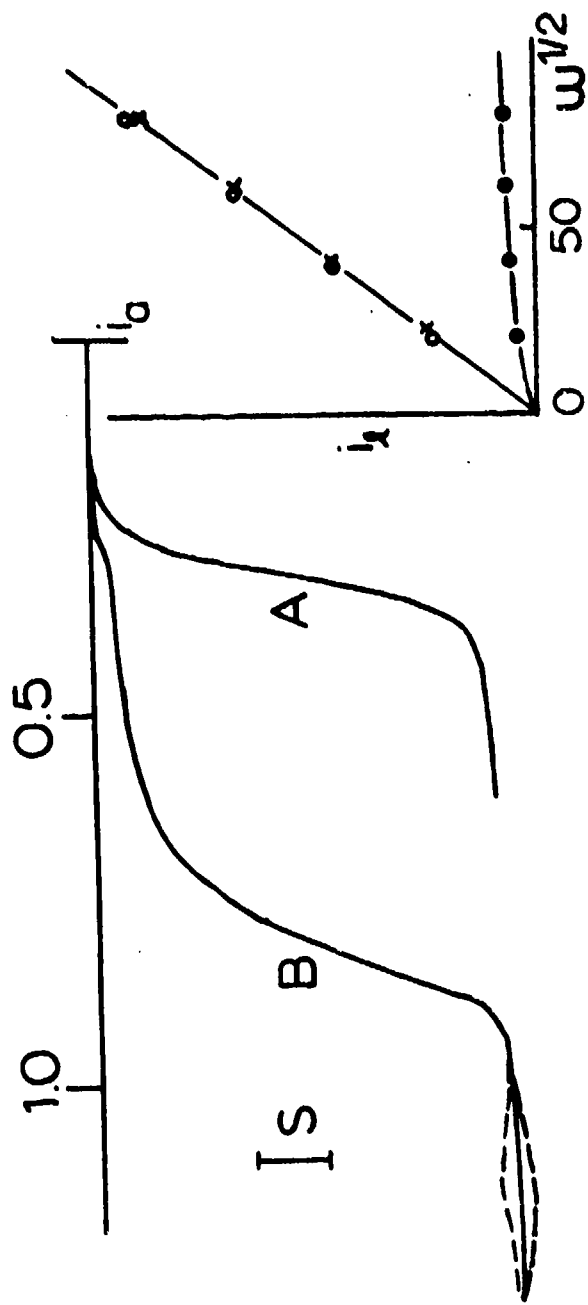
50

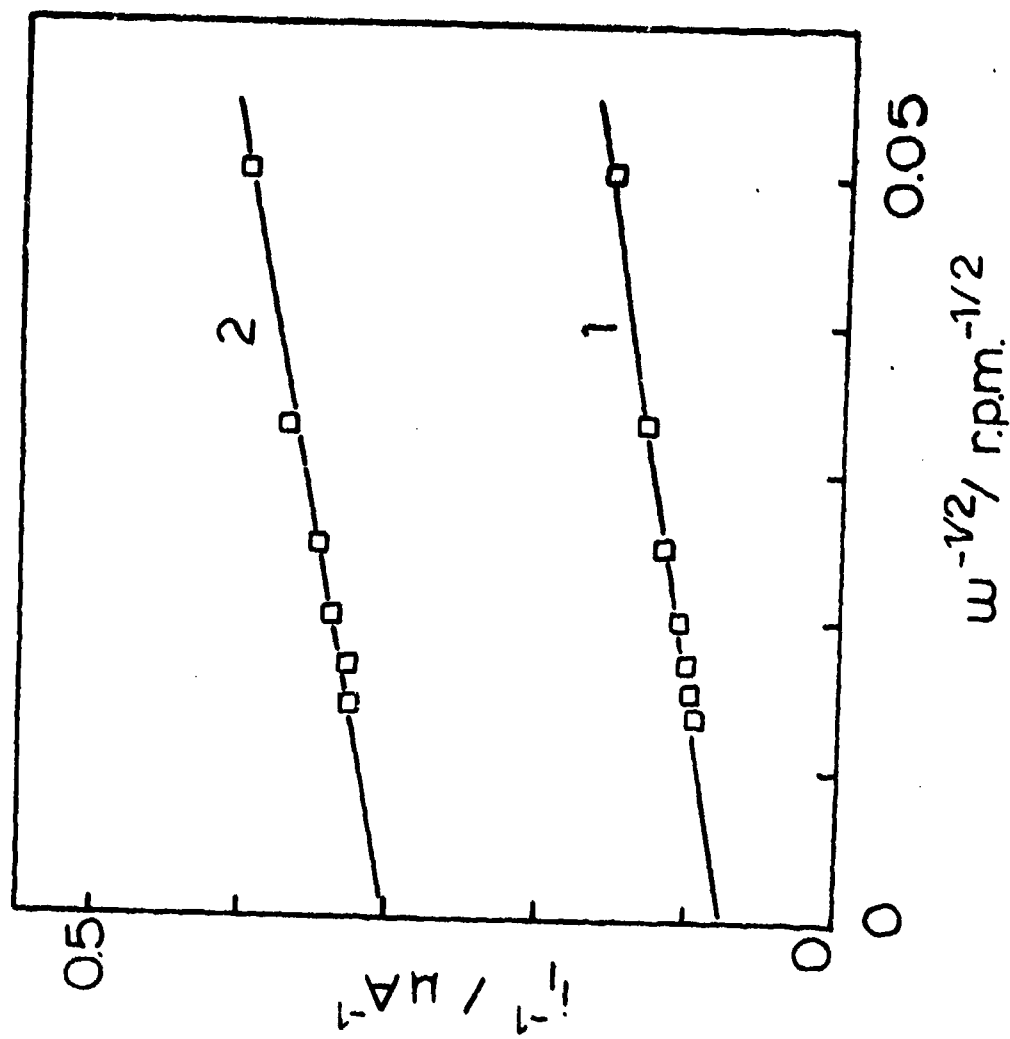
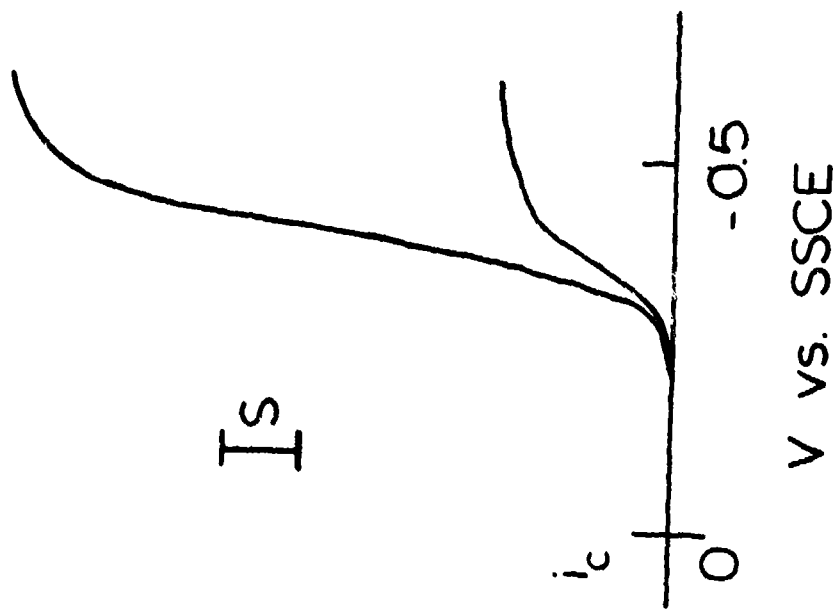
$\omega^{1/2} / (\text{rpm})^{1/2}$

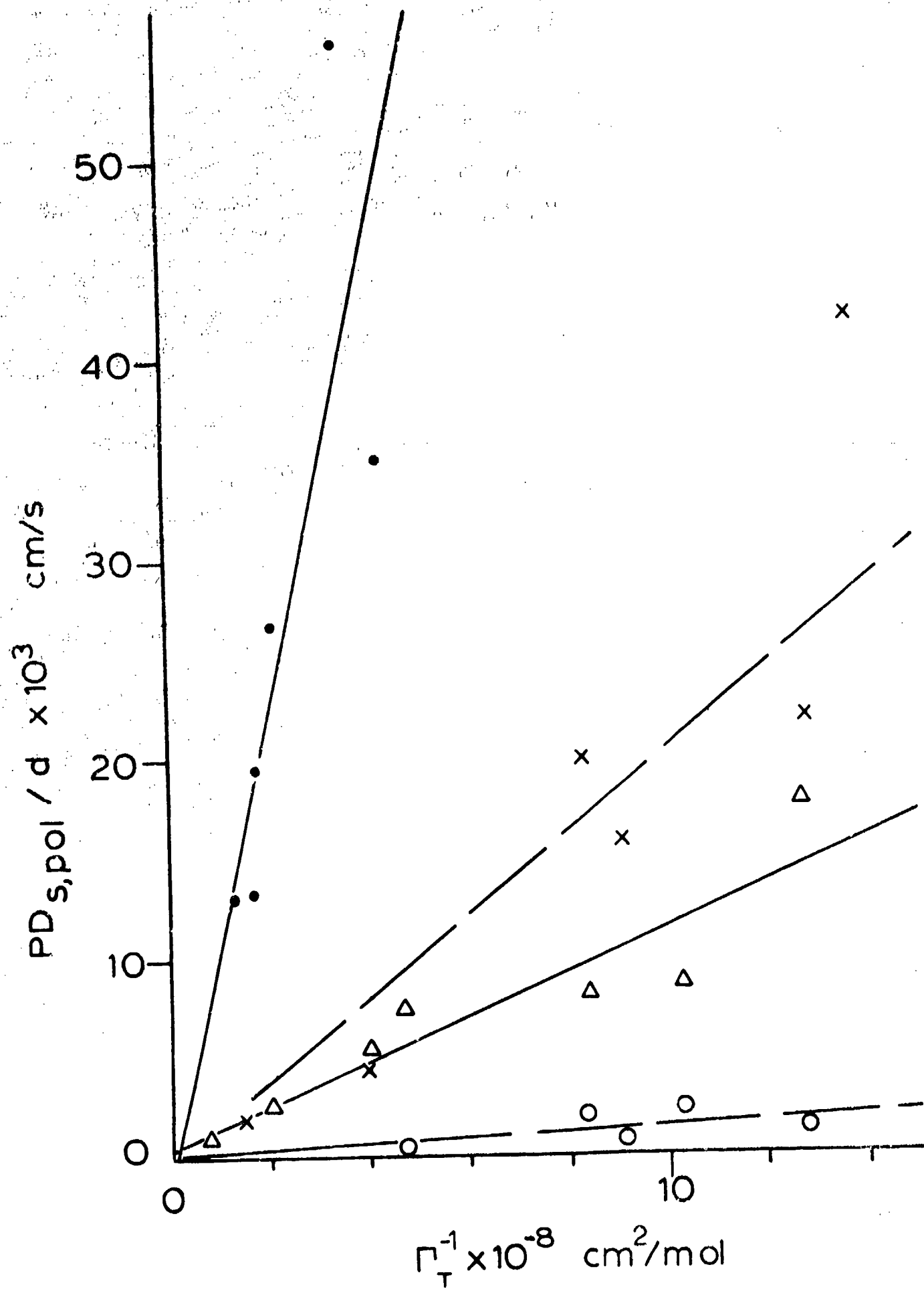




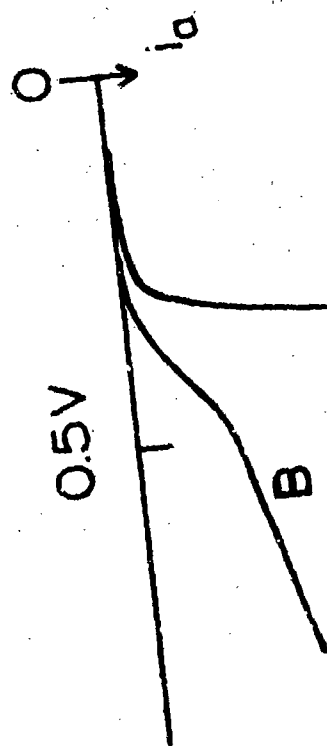
V vs. SSCE



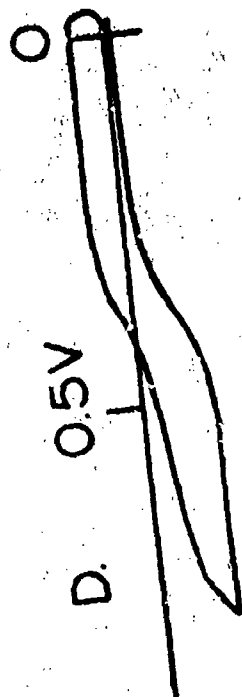
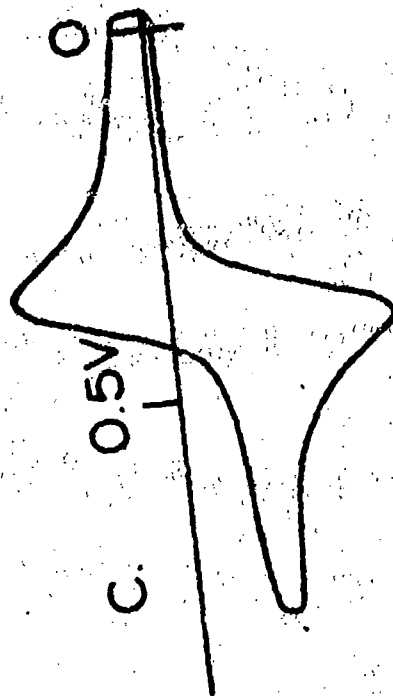




V vs. SSCE



I_s



V vs. SSCE

